Nasal tissue-resident memory CD4$^+$ T cells persist after influenza A virus infection and provide heterosubtypic protection

Authors: Nimitha R. Mathew[1,*], Romain Gailleton[1], Lydia Scharf[1], Karin Schön[1], Anneli Strömberg[1,2], Nils Lycke[1], Mats Bemark[1,2,3], Ka-Wei Tang[4,5], Davide Angeletti[1,6,*]

Affiliations:

[1]Department of Microbiology and Immunology; Institute of Biomedicine; University of Gothenburg; Gothenburg; Sweden.

[2]Department of Clinical Immunology and Transfusion Medicine, Sahlgrenska University Hospital, Gothenburg, Sweden

[3]Department of Translational Medicine – Human Immunology, Lund University, Malmö, Sweden

[4]Department of Infectious Diseases, Institute of Biomedicine, University of Gothenburg, Gothenburg, Sweden

[5]Region Västra Götaland, Sahlgrenska University Hospital, Department of Clinical Microbiology, Gothenburg, Sweden

[6]SciLifeLab, University of Gothenburg, Gothenburg, Sweden

*Corresponding authors. Email: nimitha.mathew@gu.se; davide.angeletti@gu.se

Abstract:

CD4 tissue-resident memory T (CD4 TRM) cells are crucial adaptive immune components involved in preventing influenza A virus (IAV) infection. Despite their importance, their physiological role in the upper respiratory tract, the first site of contact with IAV, remains unclear. Here, we find that, after IAV infection, antigen-specific CD4 TRM persist in the nasal tissue (NT) compartment and play a prime role in local viral clearance. Single cell RNA sequencing analysis reveals that NT CD4 TRM are heterogeneous and transcriptionally distinct as compared to their lung counterparts. Mechanistically, we demonstrate that the CXCR6-CXCL16 axis is involved in CD4 TRM residency in the NT. Furthermore, we show that the NT of mice and humans contains a high frequency of IL-17-producing CD4 TRM that aid in local viral clearance and in reducing tissue damage. Collectively, our results support a robust physiological role for nasal tissue CD4 TRM in preventing IAV infection.

Main Text:

INTRODUCTION

Influenza A virus (IAV) continues to pose a threat to society by causing yearly infections, deaths and providing a fertile ground for opportunistic bacterial infections[1]. Seasonal vaccines elicit antibodies against the immunodominant surface glycoprotein hemagglutinin (HA) which is, however, prone to antigenic drift. Therefore, vaccines show limited effectiveness and need to be updated annually [2]. In addition, there is a hovering possibility of pandemics caused by the recombination of animal and human viruses[3]. Under such circumstances, antibody-mediated protection is mostly futile. However, memory T cells recognize IAV internal proteins which are relatively conserved across different strains[4], thus mediating heterosubtypic responses.

Among the memory T cells, tissue resident memory T cells (TRM) are gaining traction as a 'ready to deploy' memory wing that is formed at the site of infection and hence acts as a barricade before the pathogens reach the circulation or lymphoid organs for the effector memory or central memory T cells to act[5]. Indeed, during IAV infection, both CD4 TRM and CD8 TRM in the lungs protect against heterologous viruses [6, 7]. Compared to CD8 TRM, CD4 TRM are still understudied, despite their multifunctionality. They can mediate viral clearance, act by direct cytotoxicity on virus-infected cells, guide the formation of IAV-specific lung CD8 TRM and orchestrate local B cell responses [7, 8, 9, 10, 11]. Specifically, lung CD4 TRM are diverse and exhibit different functions depending on their antigenic specificity. For example, two subsets of IAV NP (nucleoprotein)- specific lung CD4 TRM were recently identified: $T_{RM}1$ which are Th1 like, and T follicular helper like cells (T_{RH}) which are involved in promoting local antibody response and delivering help to local CD8 T cells [8, 9]. On the other hand, M2e (ectodomain of virus matrix protein)-specific lung CD4 TRM produce mostly IL-17 and protect against tissue injury during IAV infection[12]. However, our knowledge about diversity of CD4 TRM, in other tissues relevant for respiratory viral infection, is still limited.

In this context, the upper respiratory tract (URT) is the port of entry for any inhaled pathogen and the first site of contact with our immune cells. The immune system within the mouse URT is a complex network of draining cervical lymph nodes (cLN), nasal-associated lymphoid tissue (NALT) and immune cells dispersed within the nasal epithelium outside the NALT[13, 14] (referred as nasal tissue). The NALT is the site for the recall expansion of memory T cells and priming of naïve T cells, whereas cLN act as a priming site [15, 16]. Increasing evidence suggest that protective CD4 TRM are generated during bacterial and SARS CoV-2 infection in the URT

[10, 17, 18, 19, 20, 21, 22, 23]. Nevertheless, the cues needed for URT CD4 TRM formation and tissue residency remain elusive. For IAV, a few studies have demonstrated the protective role of URT CD8 TRM in reducing viral burden and transmission [14, 24, 25]. Surprisingly, despite the importance of CD4 TRM and the extensive spread of IAV, the role of IAV-specific CD4 TRM in URT has not been investigated.

Here, we investigate antigen-specific CD4 TRM within the URT of IAV-infected mice and healthy human volunteers. Importantly, we demonstrate that CD4 TRM formed in the nasal tissue (NT) of URT and protected upon heterologous IAV infection. Furthermore, we discover transcriptional differences between TRM populations in NT *vs* lungs and define factors required for the formation of antigen-specific CD4 TRM in the NT. Our data provide a comprehensive characterization of previously unexplored, protective IAV-specific CD4 TRM cells that reside in the URT.

RESULTS

IAV infection generates long-lived antigen specific CD4 TRM in the nasal tissue

To assess whether IAV-specific CD4 TRM arise in the URT, we transferred splenic CD4 T cells derived from Ovalbumin (OVA)- specific OT-II T cell receptor (TCR) transgenic mice ($CD45.1^+$ or $tdtomato^+$) to congenic C57BL/6J ($CD45.2^+$) mice. Subsequently, we infected the mice with mouse-adapted IAV strain, PR8 H1N1 expressing $Ova_{323-339}$ peptide intranasally (i.n.) and examined both NALT and NT for Ova-specific CD4 TRM (OT-II CD4 TRM) on day 30 post infection. We used lungs as a positive control because IAV specific CD4 TRM are well known to form in lungs [7]. Throughout all our experiments, we administered fluorochrome-conjugated CD4 antibody intravenously (iv) 5 minutes before sacrifice to distinguish CD4 T cells in the tissue from those in the vasculature (Fig 1A). CD4 memory T cells were identified as $CD3^+$, $CD4^+$, $CD44^+$, $CD62L^-$. We differentiated CD4 TRM from their circulating counterparts as CD4 iv^- and $CD69^+$ (Fig S1A). CD69 is a well-known tissue retention molecule that prevents egress of T cells from the tissue[26, 27]. OT-II CD4 TRM were present in the NT at higher frequency than lungs. Interestingly, we found less OT-II CD4 TRM in the NALT, confirming their role as an inductive site (Fig 1B-C).

To localize OT-II CD4 T cells anatomically, within the URT, we isolated, fixed and decalcified heads of PR8-OVA infected mice on day 30 post infection. OT-II CD4 T cells were found throughout the nasal chamber, including the olfactory epithelium (OE) lining the dorsal medial meatus, respiratory epithelium lining the nasal septum, maxilloturbinates (MT) and NALT (Fig 1D). Given the localization of OT-II CD4 T cells in the epithelium of the NT, we examined the expression of CD103, an integrin involved in the adhesion of T cells to E-cadherin on epithelial cells. CD103 is often associated with CD8 TRM[27, 28, 29] but its association with CD4 TRM in the respiratory tract has not been fully elucidated in mice. Indeed, CD103 was poorly expressed on lung CD4 TRM in comparison to NT CD4 TRM (5% vs 22%) (Fig 1E-F, Fig S1B). Apart from CD103, we analyzed NT CD4 TRM for the expression of CD11a, a ubiquitous residency marker for TRM [7, 27]. Nearly all OT-II CD4 TRM in the NT and lungs expressed CD11a (Fig 1E-F, Fig S1B).

Having demonstrated that NT CD4 TRM are established in a transfer model, we wanted to verify whether they would also form when precursor frequency is at physiological numbers. Hence, we took advantage of MHC-II tetramers, presenting immunodominant peptides I-A^b HA_{91-107} and I-A^b $NP_{306-322}$[30]. To follow the kinetics of antigen specific CD4 TRM, we infected

mice with PR8 and harvested the lungs and NT at several time points (Fig 1G). We found that I-A^b HA_{91-107} tetramer$^+$ and I-A^b $NP_{306-322}$ tetramer$^+$ CD4 TRM arose as early as 10dpi. The number of tetramer$^+$ CD4 TRM declined from day 10 to day 30. Although, there was a steady decrease in tetramer-specific CD4 TRM in NT and lungs, we could still detect antigen-specific CD4 TRM in the NT on 120 dpi in most of the mice, which is in agreement with the fact that CD4 TRM are considered stable[31] (Fig. 1H-I, Fig S1C).

IAV-specific CD4 TRM in the lung are self-sustaining, without being replenished from the lymphoid reservoirs[31]. To determine the crucial time window where the CD4 T cells that are poised to become CD4 TRM enter the NT, we treated mice with fingolimod (FTY720), using 10 days time windows, after PR8 infection. FTY720 is a known S1PR1 inhibitor that prevents the egress of lymphocytes from lymph nodes[32]. We found that FTY720 treatment did not affect the absolute numbers of I-A^b $NP_{306-322}$ tetramer$^+$ CD4 TRM in comparison to those in the untreated control group at any particular time window (Fig S1D). We reasoned that naive CD4 T cells may either be already present, arrive very early or continuously replenish the NT. To test these alternatives, we treated the mice daily with FTY720 from 24h pi to 29 dpi with a resting period of one day after every 5 days of treatment. Intriguingly, long-term FTY720 treatment did not affect the CD4 TRM in the NT, suggesting that these cells might be locally generated and self-sustaining (Fig S1E-F).

CD4 TRM are established in the NT after vaccination and depend on the presence of cognate antigen

After revealing that IAV infection gave rise to CD4 TRM in NT, we wanted to establish whether i.n. vaccination had a similar effect. To this end, we utilized CTA1-3M2e-DD, which contains 3 tandem repeats of M2e linked to CTA1-DD adjuvant, as immunogen. M2e is highly conserved among IAVs and immunization with CTA1-3M2e-DD has been shown to induce M2e specific lung resident CD4 T cells that protect against lethal IAV challenge in mice[33, 34]. We chose to use BALB/c rather than C57BL/6 for immunization as CTA1-3M2e-DD induces poor M2e specific T cell response in C57BL/6[34]. To maximize the formation of CD4 TRM in NT, we modified the immunization protocol and reduced the volume to 5µl. We vaccinated mice with CTA1-3M2e-DD three times and evaluated the M2e specific CD4 TRM response on day 30 (Fig 1J). Similar to response after infection, we found that I-A^d $M2e_{2-17}$ tetramer$^+$ CD4 TRM robustly formed in the NT (Fig 1K-L).

The presence of cognate antigen has a tissue dependent role in the formation of TRM. Indeed, while cognate antigen is a crucial factor for lung CD8 TRM formation[35] it is not required by CD8 TRM in NT[14]. Thus, we sought to assess the cognate antigen requirement for NT CD4 TRM formation. We generated effector tdtomato$^+$ OT-II T cells *in vitro* and transferred them to C57BL/6 mice that were infected with either PR8 or PR8-OVA two days prior [14] (Fig 1M). In this model, even though effector OT-II cells can access the NT in both PR8 and PR8-OVA infected groups, we found that OT-II CD4 TRM were retained in the NT of the PR8-OVA-infected mice only (Fig 1N-O). This was also observed for lung CD4 TRM (Fig S1G-H). Our results demonstrate that cognate antigen is required for the conversion of effector OT-II T cells to OT-II CD4 TRM in respiratory mucosal tissues.

In summary, we found that IAV-specific CD4 TRM are generated and persist in the NT following infection and intranasal vaccination.

NT CD4 TRM engage in local viral clearance upon heterologous viral challenge.

Rapid and efficient response to viral re-infection is a key feature of memory T cells, including CD4 TRM. Upon recognition of their specific antigen, memory T cells reactivate and produce cytokines, some of which have a direct impact on virus-infected cells while others influence the recruitment of other immune cells[36]. To detect the IAV-specific response in NT CD4 TRM, we stimulated NT and lung cells containing CD4 TRM, from PR8-infected mice, with IAV-derived nucleoprotein (NP) peptide pool. Compared to unstimulated controls or naïve NT CD4 TRM, stimulated NT CD4 TRM produced IFN-γ and IL-2, but less TNF. In general NT CD4 TRM harbored lower frequency of cytokine producing cells than lung CD4 TRM (Fig 2A-B and Fig S2A). Lung and NT CD4 TRM had a similar immunodominance hierarchy with regards to response towards different IAV-derived peptides (Fig S2B). To exclude the possibility that NT CD4 TRM had a more exhausted phenotype we measured PD-1 expression. Still, CD4 TRM from both organs had a similar frequency of PD-1^{+} CD4 TRM indicating this was not the case (Fig 2C-D, Fig S2C) but suggesting a role for PD-L1-PD1 axis in CD4 TRM regulation, similarly to what was described for IAV-specific CD8 TRM[37]. Surprisingly, even though NT CD4 TRM had overall lower frequency of cytokine producing cells, ICOS expression, a T cell co-stimulatory molecule [38, 39], was higher in NT CD4 TRM in comparison to lung CD4 TRM (Fig 2C-D, Fig S2C).

CD4 TRM promote viral clearance by recruiting B cells, CD8 T cells and innate cells and by exerting direct cytotoxic effects on virus-infected cells[36]. Given that NT CD4 TRM displayed an IAV-specific response, we wanted to determine their involvement in local viral clearance during a heterosubtypic challenge. To test this, we infected mice with PR8 and challenged them with heterologous X31 H3N2 virus on day 30 post primary infection and measured the viral titer in NT on day 3 post X31 infection. To rule out the contribution of circulating lymphocytes, we treated the mice with FTY720. In addition, we depleted either CD4 T cells, CD8 T cells or both (Fig 2E). In the absence of any intervention, the secondary infection was cleared from the NT by cross-reactive T cells (Fig 2F), as PR8-antibodies did not neutralize X31 (Fig S2D). Surprisingly, depletion of CD8 T cells did not affect the viral clearance in the NT (with or without FTY720 administration) bolstering the role of CD4 TRM in viral control. Conversely, CD4 T cell depletion severely impaired local viral clearance, with viral titers similar to those of the mice that did not undergo a primary infection (Fig 2F and Fig S2E).

Taken together, our findings revealed that NT CD4 TRM respond to IAV by producing cytokines and are indispensable for local viral clearance during heterosubtypic infection.

CD4 TRM in the lungs and NT are heterogeneous, but Th17 cells are prevalent in the NT.

Having identified the dynamics and role of NT CD4 TRM, we wanted to investigate the transcriptional differences between total and antigen-specific CD4 TRM in NT *vs* lungs. Therefore, we performed scRNA-seq together with scTCR-seq at 30 dpi. Mice were injected with CD4 antibody i.v. 5 minutes before sacrifice and total CD4 TRM, I-A^{b} HA$_{91\text{-}107}$ tetramer^{+} and I-A^{b} NP$_{306\text{-}322}$ tetramer^{+} CD4 TRM sorted from NT and lungs of mice (Fig. 3A). Furthermore, we sequenced a small proportion of all live cells, which were CD4^{-}. To maximize the number of cells and samples that could be loaded simultaneously, different samples were labeled with hashtag antibodies. Data from all mice and organs were integrated, processed, and visualized on a two-dimensional UMAP (Fig 3B). T cell subpopulations were assigned based on well-known markers and gene signatures (Fig 3C-D and Fig S3A). The major T cell subpopulation was, as expected given the intracellular viral infection, Th1 cells (Fig S3B) defined by a well-established signature[40], *Ifng* and *Cxcr3*. Cytotoxic CD4 T cells were present

in both organs and defined by *Nkg7*, *Fasl*, *Ccl4*, *Ccl5* and a CD4 cytotoxic signature[41]. We were unable to properly define a third major cluster, C.3: this cluster harbored several mitochondrial genes, even though all mitochondrial genes were regressed out and did not contribute to the clustering. Therefore, we believe these cells to be either senescent/dying cells or highly proliferative cells. Tfh cells were generally more prevalent within lungs (Fig S3B), consistent with a possible role in supporting ectopic GC in iBALTs. Based on their transcriptional profile they were separated into two clusters, named Tfh.1 and Tfh.2. Tfh.1 were Tfh cells with strong expression of *Tnfsf8*, *Bcl6*, and a signature previously associated with Tfh [40]. Nevertheless, Tfh.2 had higher expression of other Tfh-associated genes such as *Tox*, *Slamf6* and *Pdcd1*. C.5 cells expressed several transcription factors, *Cd40lg* but also had strong expression of genes involved in regulation of NF-kB signaling (*Nfkbia*, *Nfkbid*, *Nfkbiz*). This cluster has been previously reported and suggested to include cells which are poised to rapidly respond to secondary infections by producing cytokines [42, 43]. Quiescent memory cells were slightly more prevalent within NT and characterized by the expression of several long non-coding RNAs (including *Malat1*)[44, 45] and low ribosomal gene expression. A small proportion of our CD4 TRM was naïve-like T cells expressing *Ccr7*, *Sell* and *Klf2* [46]. Furthermore, we identified Tregs strongly expressing *Foxp3* and Treg-signature[47]. Early activated cells were defined based on the expression of genes linked with migration within the tissue, such as *Gpr183*[48], and signaling receptors such as *Ms4a4b*[49] suggesting an overall movement within the tissue but also modulation of T cell activation. NKT cells and IFN responsive cells were clearly identified by their distinctive signatures: the former expressed *Klrd1*, *Klrk1*, *Klrb1c*[50, 51] and other cytotoxic genes (*Nkg7*, *Fasl*)[52, 53] while the latter was enriched for Interferon stimulated genes (*Isg15*, *Ifit3*, *Ifit1*) and similar signature, previously identified in human CD4[54]. Strikingly, Th17 cells, expressing *Rorgc*, *Il17a*, *Tmem176a*, among others, were much more abundant within NT[54] (Fig S3B). Finally, we were able also to identify several endothelial and epithelial airway cells clusters, from the live cell fraction devoid of CD4 T cells.

Overall, our scRNASeq analysis highlighted a remarkable diversity and variety of CD4 TRM subpopulations in both lungs and NT. While Th1 and cytotoxic CD4 T cells made up almost 50% of the total TRM in both lungs and NT, consistent with an intracellular viral infection, their relative proportions were similar between organs (Fig. S3B). Interestingly, IAV infection did not appear to majorly reshape the CD4 TRM landscape in terms of the abundance of cell type (Fig S3C). Therefore, to confirm our results and limit our analysis to influenza-specific cells, we subsetted the CD4 to include only the tetramer$^+$ cells. Indeed, this did not change the proportion of CD4 TRM, confirming an increased abundance of both HA$^+$ and NP$^+$ Th17 cells within the NT, while these cells were almost absent in lungs (Fig 3E and Fig S3D). By visualizing the distribution of HA$^+$ and NP$^+$ cells as density plot we established that antigen-specific cells differentiated into almost all CD4 TRM subsets, except for Th17 in the lungs. However, the density distribution in NT was dramatically different between the two proteins, with NP$^+$ being mostly Th17 and Th1 while HA$^+$ included also included many cytotoxic and Tfh CD4 TRM cells (Fig 3E and Fig S3D).

CD4 TRM within the NT exhibit a distinct transcriptional profile, compared to lungs.

The power of the single cell approach is that it allows transcriptional differences to be compared between the same CD4 TRM subtypes, depending on the organ. Therefore, we performed differential gene expression (DEG) analysis for each cell subpopulation and visualized the results with both heatmap and volcano plots (Fig S4A-B). As expected, the majority of CD4

TRM subpopulations exhibited similar gene expression between organs, however Th1, Cytotoxic CD4, Tfh.1 and Th17 clusters demonstrated significant differences. For Th1, lung cells had higher expression of *Ccr2*, a chemokine receptor previously linked with pulmonary homing[55, 56], *Ctla4* but also *Ifng*, *Nfkbia* suggesting a more active and productive phenotype, compared to that of their NT counterpart, as we also observed (Fig 2A-B). On the other hand, NT Th1 were enriched for other essential transcription factors such as *Crem*, *Taf7* which are involved in cytokine production[57, 58] and *Xcl1*, which promotes Treg differentiation[59], suggesting overall a more immune-suppressive state. Cytotoxic CD4 had similar pattern with *Ccr2* and genes associated with a more active phenotype expressed in the lungs. Interestingly, NT CD4 TRM in this cluster upregulated several chemokine receptors including *Cxcr6* and *Ccr8* and many other factors previously associated with T cells at mucosal sites (such as *Spp1* and *Penk*)[60, 61]. Remarkably *Cxcr6* was also significantly upregulated in NT Tfh.1 and Th17 clusters. In addition, Tfh.1 NT cells shared also *Tff1* and *Xcl1* upregulation with other clusters, while NT Th17 exhibited increased *Crem* and *Nr4a2* expression.

In summary, several CD4 TRM subpopulations displayed differential gene expression between lungs and NT with the lung cells showing a more activated phenotype and *Ccr2* expression, consistent with their localization. Conversely NT CD4 TRM expressed genes commonly associated with T cells at mucosal sites and with an immune-dampening phenotype, with several clusters also expressing the chemokine receptor *Cxcr6*.

Expanded clonotypes have multiple fates and populate both lungs and NT.

Having identified differences between CD4 TRM residing in different organs we wanted to investigate whether T cell clones were compartmentalized or shared between them. A caveat of our experimental procedure is that we had to pool several mice to obtain sufficient numbers of antigen-specific cells and, therefore, we were not able to define clonality at the single mouse level. However, a previous study suggested that $CD4^+$ T cell responses are largely private even for a single viral-peptide specificity[40]. Consistent with the notion of a largely private response we did not detect any exaggeratedly expanded T cell clones, with only 5 families with more than 30 members. Expanded clones were distributed across the majority of CD4 TRM subpopulations within the lungs, except for Naïve, Treg, NKT and Th17 which were populated mainly by single clones (Fig 4A); conversely, NT exhibited relatively higher clonal expansion within Th17. When focusing only on antigen-specific clones, we detected a very similar pattern of clonal expansion (Fig S5A). To visualize the specificity, organ and subpopulation distributions, we plotted the top 34 expanded clones (Fig 4B). We confirmed the pattern of expansion and that the majority of expanded clones were shared among several subpopulations but also between organs. Validating our tetramer sorting approach, clones were either HA or NP specific, however, in many cases, we did not sort all clones within the same family, as also expected. Substantiating the private nature of TCR response was the fact that many of the NP expanded clones had similar, but not identical, CDR3 sequences (Fig 4B). This suggests that certain TCRs had higher affinity for NP peptide but stochastic variations, not altering binding, were present between mice. Indeed, analysis of paired TCRa-TCRb usage demonstrated a strong bias in NP responses for TRAV6-7_TRBV3 for both lungs and NT (Fig S5B). By visualizing with a bubble plot, in which the size of the bubble is proportional to the clone size, we revealed that many of the more expanded, antigen-specific clones in the lungs were also shared to the NT (Fig 4C). This points toward a common origin within the same lymph nodes and subsequent migration to tissues of residency. Finally, to determine whether certain clonotypes were more

prone to direct CD4 TRM toward a certain fate we utilized the "clonotype bias" measure introduced by Andreatta et al.[40] and implemented within the scRepertoire package[62]. The analysis revealed that the majority of clonotypes were largely unbiased with few exceptions (Fig 4D). Interestingly, clonotype bias strongly correlated with being organ-specific (Fig 4D-E). For instance, the third largest clone was present only in the lungs and over 60% of its members belonged to the Tfh.2 cluster (Fig 4D-E). Likewise, the only clone found only in NT had just shy of 50% of its members belonging to the early activated CD4 TRM group. However, the most expanded clones were generally not biased, despite having a strong prevalence of Th1 and Tfh.1 cells (Fig 4F). The tendency of the few biased clones to be organ specific could suggest local proliferation and expansion.

Combined TCR analyses unveiled how most CD4 TRM clonotypes can differentiate into multiple fates and reside in both lungs and NT. However, there were few clones that were tissue-specific, and they tended to be biased toward one CD4 T cell subtype.

CD4 TRM rely on the CXCR6-CXCL16 axis for recruitment to the NT

Given that *Cxcr6* was highly expressed in several NT clusters (Fig S4A-B) we further explored the mechanistic involvement of this chemokine receptor in the migration of effector CD4 T cells to the NT. First, we confirmed *Cxcr6* to be the most interesting candidate as it was more highly expressed in NT CD4 TRM than in lung CD4 TRM (Fig 5A-C). In particular, the clusters of cytotoxic CD4 T cells, Tfh.1, Th17, Treg, early activated and Tfh.2 displayed higher expression of *Cxcr6* in NT (Fig 5B). CXCR6 is known to be predominantly expressed in CD8 TRM rather than circulating CD8 T cells [63]. Similarly, we found high CXCR6 expression in CD4 TRM and low expression in CD4 effector memory T cells (TEM iv$^+$) of IAV-infected mice (Fig 5D). While CXCR6 expression was greater in infected NT than lungs, its expression was similar to that of NT CD4 TRM in naïve mice (Fig 5D). This may seem surprising, however, by definition, TRM are not naïve cells and therefore their presence in NT has been triggered by a previous insult. Furthermore, we also found higher CXCR6 expression among antigen specific OT-II TRM in NT *vs* lungs (Fig 5E-F).

Within the lungs, CXCR6 is essential for the positioning of CD8 TRM in the airways but not in the lung interstitium after IAV infection[64]. To determine whether CXCR6 is required for the establishment of CD4 TRM in the NT, we generated WT-*Cxcr6*$^{-/-}$ bone marrow (BM) chimeras. To do this, we lethally irradiated congenic C57BL/6 (CD45.1$^+$) (recipient) to deplete the host bone marrow and reconstituted them with equal numbers of tdtomato$^+$ WT BM (CD45.2$^+$) and tdtomato$^-$ *Cxcr6*$^{-/-}$ BM (CD45.2$^+$) (Fig 5G). Blood chimerism was verified on day 67 post BM transfer, with almost 90% of the leukocytes being donor-derived. Interestingly, we detected a higher frequency of *Cxcr6*$^{-/-}$ leukocytes in the blood (Fig S6A). On the 70th day post BM transfer, we infected the mice and analyzed organs at day 30 post infection. Remarkably, CXCR6 was required for lodging total and I-A^b NP$_{306-322}$ tetramer$^+$ CD4 TRM in both NT and lungs, as we observed a reduced frequency of *Cxcr6*$^{-/-}$ CD4 TRM in comparison to WT CD4 TRM in both compartments (Fig 5H-J). Surprisingly, we found that 6 out of 13 chimeric mice did not develop I-A^b NP$_{306-322}$ tetramer$^+$ CD4 TRM in the NT, from neither WT nor KO cells (Fig 5J). We speculate that this may be due to a generally low level of donor T cell chimerism achieved at the NT in comparison to that in the lungs (Fig S6B). The finding that NT CD4 TRM are not easily depleted or replenished, consolidate our data about longevity of these cells, i.e. that once they are formed and reside in the NT they will persist for long. Moreover, we detected an increased accumulation of *Cxcr6*$^{-/-}$ CD4 T cells in the blood, spleen, lung-draining mediastinal

lymph nodes (mLN) and URT-draining cervical lymph nodes (cLN), confirming the hypothesis that *Cxcr6*$^{-/-}$ CD4 T cells have migratory defects and/or they are not retained at the tissue (Fig S6C).

CXCL16 is the only known ligand for CXCR6: it exists in both transmembrane and soluble forms and acts as an adhesion molecule and a chemoattractant for leukocytes[65, 66]. In murine lungs, CXCL16 colocalizes with Epcam and its expression is restricted to the large airways lining the lungs[64]. To substantiate our results, we investigated CXCL16 expression in NT by microscopy and demonstrated that CXCL16 is expressed in the NT of PR8-OVA infected mice and some OT-II CD4 TRM localize near CXCL16 (Fig 5K). Finally, to examine the contribution of CXCL16 to the recruitment of effector CD4 T cells to the NT and lungs, we treated PR8-infected mice with α-CXCL16 antibody (Fig 5L). α-CXCL16 treatment significantly reduced the frequency and number of I-A^b NP$_{306-322}$ tetramer$^+$ CD4 TRM retained in the NT and, to a lesser extent, in the lungs (Fig 5M-N).

Altogether, we demonstrated that CXCL16 production by airway cells and CXCR6 expression on CD4 T cells are required for the recruitment of CD4 effector memory T cells to respiratory mucosal tissues and subsequent establishment of TRM.

Healthy humans harbor IAV-responsive CD4 TRM in the nasal mucosa.

Given the importance of IAV-specific CD4 TRM in the NT of mice, we wanted to investigate whether a similar population exists in healthy human adults. As every individual is exposed to IAV by the age of three[67], healthy adults must have undergone several symptomatic and asymptomatic infections and we hypothesized that they should maintain IAV-specific CD4 TRM in their NT. The recruited subjects did not have any respiratory infection or symptoms in the two weeks prior to the study, to avoid contamination from recently activated CD4 T cells. We collected nasopharyngeal swab and peripheral blood mononuclear cells (PBMC) and analyzed NT CD4 TRM (CD3$^+$CD4$^+$CD45RA$^-$CCR7$^-$CD69$^+$) and CD4 effector memory T cells (TEM) (CD3$^+$CD4$^+$CD45RA$^-$CCR7$^-$) by flow cytometry[68] (Fig S7). Interestingly, all the subjects had CD4 TRM in the NT in varying numbers. When we analyzed both the compartments, we found that NT CD4 TRM included CD103 (18%) and CXCR6 expressing cells (23%) while CD4 TEM barely expressed them, similar to the findings in mice (Fig 6A-B).

A longitudinal study on SARS-CoV-2 vaccinees who had breakthrough infections showed functional NT T cells, specific for SARS-CoV-2 that proteins that persisted for ≥140 days[19]. Given the relatively long lifespan of NT CD4 T cells, we wanted to examine whether healthy adults retained IAV-specific NT CD4 TRM, acquired by encountering IAV at some timepoint in life. To do that, we stimulated PBMC and NT cells with IAV peptide pools derived from the internal proteins NP and M1 (Matix protein 1) and assessed cytokine expression. We found that PBMCs CD4 TEM from ~79.5% of the subjects responded to stimulation to secrete IFN-γ (Fig 6C). Conversely, we did not detect an IFN-γ response in NT CD4 TRM after stimulation. Furthermore, we found poor TNF response in both NT and PBMCs (Fig 6C). scRNA-seq revealed high frequency of Th17 cells in NT (Fig 4E), hence we tested for IL-17a expression in stimulated cells. Intriguingly, NT CD4 TRM contained IL-17a expressing cells whose frequency increased, after stimulation, in 63.2% of the individuals. Little to no IL-17a expression was detected in PBMCs before or after stimulation (Fig 6C-E).

Overall, our data demonstrate that human NT CD4 TRM share important features with mouse CD4 TRM, such as the expression of CD103 and CXCR6. Moreover, NT of healthy individuals is populated by IAV-specific Th17 CD4 TRM.

NT Th17-CD4 TRM promote viral clearance and dampen tissue damage

Given the abundance of Th17 CD4 TRM in NT of mice and human, we wanted to further delineate their functional role. First, we confirmed that PR8-infected mice carried IAV-specific Th17 CD4 TRM in NT. Therefore, we stimulated lung and NT cells with a single immunodominant NP peptide ($NP_{306-322}$) and assessed the intracellular expression of IL-17a as a measure of Th17 response. We used $NP_{306-322}$ as this was the same peptide, loaded into tetramers, used to sort CD4 TRM for scRNA sequencing. Consistent with all our data, we found that only NT, but not lung, CD4 TRM from PR8 infected mice expressed IL-17a. Surprisingly, IL-17a production was stimulation-independent although infection-dependent (Fig 7A-B).

Th17 cells recruit neutrophils, B cells, transport secretory IgA to the mucosal sites and protect the hosts in an antibody independent manner during IAV infection[34, 69, 70, 71]. Conversely, detrimental effect of Th17 was also reported as an intranasal immunization triggered Th17 population that caused increased morbidity in mice[72]. To examine whether NT Th17 CD4 TRM were protective, we utilized *CD4*^{Cre}*Rorc*$^{fl/fl}$ (CD4-specific Th17 KO) and *CD4*^{Cre}*Rorc*$^{fl/wt}$ (WT) mice[73]. Mice deficient in *Rorc* gene lack RORγt, a Th17 lineage-specific transcription factor, that controls the activation of IL-17A and IL-17F genes and thus lack Th17 CD4 T cells[74]. To verify the specific protective role of Th17 CD4 TRM, we infected *CD4*^{Cre}*Rorc*$^{fl/fl}$ and *CD4*^{Cre}*Rorc*$^{fl/wt}$ mice with PR8 and challenged them at day 30 post primary infection (Fig 7C). FTY720 treatment ruled out contribution of circulating lymphocytes. Indeed, CD4 Th17 KO mice had slightly higher viral titer in the NT than did WT mice on day 3 post-secondary infection (Fig. 7D). Furthermore, Th17 CD4 cells have been suggested to play a role in tissue repair and, by secreting anti-apoptotic cytokines, in dampening tissue damage[75, 76]. We performed a reinfection experiment in a similar way and enumerated apoptotic cells ($TUNEL^{+}$) in the NT upon X31 challenge (Fig 7E). Indeed, *CD4*^{Cre}*Rorc*$^{fl/fl}$ mice exhibited increased number of apoptotic cells in the NT (Fig 7 F-G).

Altogether, we confirmed that Th17 CD4 TRM dominate NT-immunity upon IAV infection. NT Th17 CD4 TRM ameliorate IAV-related pathology by controlling local viral titer and reducing tissue damage.

DISCUSSION

CD4 TRM cells are multifunctional and protective during heterologous IAV infection. The current understanding of CD4 TRM during IAV infection relies on findings from lung CD4 TRM. Surprisingly little is known about CD4 TRM at other mucosal sites, that are relevant for respiratory viral infections. Yet, the URT is the first location where IAV encounters the immune system and thus is crucial for preventing viral spread to the lungs and dampening disease severity. Therefore, CD4 TRM in the URT may be a key tool for reducing IAV disease severity. Here, we defined the phenotype and functional role of CD4 TRM residing in the nasal tissue region of the URT. We demonstrated that CD4 TRM protect against heterologous IAV by direct viral clearance and by tissue protection in the URT.

Notably, we found that antigen-specific CD4 TRM, especially the HA-specific cells are long lived. The HA^+ CD4 TRM in the NT decayed at a slower rate than CD4 TRMs in the lungs, even though they were less abundant, when quantified in absolute numbers. Surprisingly, we found that long-term FTY720 treatment, starting from 24 h post infection, did not affect the number of antigen-specific CD4 TRM in the NT. This suggests that these cells are either produced locally or that precursors arrive early, within 24 hours of infection. Thereafter, they may be maintained by homeostatic proliferation without the need for replenishment from circulation or lymphoid organs, similar to lung CD4 and CD8 TRM[31, 35]. We hypothesize that the NALT could be the main site for naïve CD4 T cell priming and expansion, seeding CD4 TRM in the NT[77]. Indeed, a recent study showed that intranasal vaccination established a CD4 T cell response within the interfollicular regions of the NALT, in turn promoting the homing of antibody-secreting plasma cells to the NT[16]. Since NALT and the surrounding NT are closely knit structures, it is possible that FTY720 treatment did not prevent the egress of CD4 TEM to the NT.

In apparent contradiction, our TCR sequencing data indicate extensive clonal sharing between NT and lung. However, NALT-activated T cells may migrate to the lungs, after activation, where they become TRM. Nevertheless, it should be noted that, while expanded lung clonal families are also found within the NT, the opposite is not true, with all clonal families in the NT with >8 members being organ specific (Fig 4C). This suggests that few cells traffic from lung draining lymph nodes to NT, but the majority do expand *in situ*. Although we cannot conclusively offer an explanation, both these phenomena may happen at the same time, thus explaining our results.

Even though effector T cells traffic to the infection site due to inflammatory cues, their establishment as TRM may or may not require the presence of antigen depending on the tissue. Antigen-dependent residency has been described for the lungs and brain[78, 79, 80, 81], but not genital tract or intestinal CD8 TRM, where the inflammatory milieu and chemokines are sufficient for their formation[82, 83]. Even in lungs, antigen-dependency can be bypassed by the introduction of adjuvants, such as zymosan, which evoke a specific inflammatory milieu [84]. Here, we demonstrated that CD4 TRM in NT require the presence of cognate antigen to be formed after IAV infection, which is the opposite of CD8 TRM [14]. Furthermore, we showed that the same held true for lung CD4 TRM. The observation in the NT highlights an interesting discrepancy regarding the minimal cues needed by different T cell types to establish residency, even within the same tissue.

Generally, CXCR6 is a chemokine receptor that is more highly expressed on CD8 T cells than on CD4 T cells[63, 85] and is well described as an essential factor for CD8 TRM seeding to the lung airways but not the lung interstitium, after IAV infection [64]. Here, using bone marrow chimeras and blocking experiments we revealed that the CXCR6-CXCL16 axis plays a role in the formation of antigen-specific CD4 TRM in both NT and lungs. Another study did not find a role for CXCR6 in the recruitment of total antigen specific CD4 T cells to the lungs of *M. tuberculosis* infected mice [86], however the establishment of TRM was not verified. Nevertheless, a recent sequencing study suggested the presence of CXCR6-CXCL16 interaction in the nasal mucosa of IAV-infected mice, using cell-cell communication analysis [87]. The authors showed CXCL16 to be expressed by monocyte derived macrophages and KNIIFE cells (Krt13+ nasal immune-interacting floor epithelial) cells. Similarly, we found that cells in the NT express CXCL16 however we did not pinpoint the cell population that express them. We

suggest two possible mechanisms by which CXCL16 could recruit CD4 TEM to the NT: either as soluble chemokine, by attracting CD4 TEM or as membrane bound, by retaining the CD4 TRM after migration [65, 66].

Functionally, NT CD4 TRM produce cytokines such as IL-2 and IFN-γ upon antigen stimulation. IFN-γ is a cytokine that protects the host by inhibiting viral entry, blocking attachment and replication and stimulating NK cells proliferation during the early phase of infection[88, 89, 90, 91]. In addition, our scRNA-seq data highlighted the presence of diverse CD4 TRM subtypes, such as cytotoxic CD4 which has had also been suggested to play a role in antiviral defense[11, 92]. In line with these mechanisms, we found that CD4 TRM are essential, while circulating memory CD4 cells are dispensable, for local viral clearance in the NT. Our results agree with previous findings demonstrating that mucosal lung CD4 TRM are better at producing IFN-γ and at protecting against IAV infection than are splenic memory CD4 T cells[7].

Interestingly, we detected a greater proportion of Th17 cells in NT CD4 TRM. Th17 enrichment was independent of both antigen specificity and infection status. In general, NT harbored a substantial proportion of CD4 memory T cells and very few naïve CD4 T cells. Th17 cells present at steady state could have formed in response to commensal microbiota of naïve mice; indeed, it is well known that commensal bacteria play an important role in mucosal immunity and tolerance induction [16, 93]. We speculate that the Th17 CD4 TRM in the naïve mice might have an immunoregulatory function similar to that of commensal-specific Th17 in the intestine[94] or they may be lodged earlier in life, in response to other external stimuli. In addition, in healthy human subjects, CD4 TRM produced IL-17 upon IAV-antigen stimulation. This strongly suggests that IAV-specific Th17 CD4 TRM are formed and persist in the NT of healthy adults for years and can be reactivated upon reinfection, similar to what was shown for SARS-CoV-2 and *B. pertussis* [19, 95]. Importantly, lung Th17 cells have been previously reported to protect from IAV infection in an antibody independent manner[34, 69, 70, 71]. The underlying mechanisms have not fully elucidated, but IL-17 can recruit Siglec-F^+ neutrophils in the nasal mucosa [10]and promote IFN-γ production[96]. Furthermore, Th17 cells themselves are plastic and can secrete IFN-γ[97]. In addition, NT Th17 cells have been shown to form during and protect against several intranasal bacterial infections[10, 98]. All these studies took advantage of *Il17a*-/- mice, which totally lack IL-17a production, and thus have not been able to determine a definitive role for CD4 Th17 cells specifically. Here, for the first time, we used a recently described conditional knockout, $CD4^{Cre}Rorc^{fl/fl}$ [73], which allowed us to exclusively dissect the contribution of Th17 CD4 T cells. We demonstrated that NT Th17 CD4 TRM play a role in viral clearance and in reducing apoptosis upon heterologous IAV infection. Accordingly, Th17 CD4 T cells are well known to produce IL-22[99], which in turn can stimulate the production of anti-apoptotic factors within airways epithelial cells[100]. Still, we cannot exclude the possibility that increased apoptosis in $CD4^{Cre}Rorc^{fl/fl}$ mice might be due to the higher viral titers, as IAV-infection itself is known to induce apoptosis [101].

Finally, given that nasal respiratory epithelium plays a major role in the transmission of airborne viruses, it is essential to focus on immunization strategies that can induce memory cells in the NT[24]. Although the current intramuscular IAV vaccines are largely effective against IAV infection, they are poor at inducing mucosal immune responses and at protecting against heterologous viruses. Our findings that intranasal CTA1-3M2e-DD immunization can induce M2e-specific CD4 TRM, along with another recent study showing that intranasal Spike vaccination generates antigen specific CD4 TRM in the NT support intranasal immunization as

an effective tool for generating functional CD4 TRM in the NT[102]. Even though relatively long lived, in comparison to CD8 TRM, strategies to overcome their gradual decay need to be developed.

Collectively, our data provide a comprehensive understanding of NT CD4 TRM that could be leveraged to design mucosal vaccines aimed at generating NT CD4 TRM providing heterosubtypic protection.

MATERIALS AND METHODS

Mice

We conducted the experiments according to protocols approved by regional animal ethics committee in Gothenburg (ethical permit numbers: 1666/19, 2230/19 3307/20 and 38/23). C57BL/6N and BALB/c mice were purchased from Janvier labs, France and Taconic Biosciences, Denmark. They were housed in the specific pathogen free animal facility of Experimental Biomedicine Unit (EBM) at the University of Gothenburg. B6.SJL-*Ptprc*^{a} *Pepc*^{b}/BoyJ (CD45.1^{+}) and B6.129P2-*Cxcr6*^{tm1Litt}/J (CXCR6$^{-/-}$) mice were purchased from the Jackson Laboratory, USA and were bred at EBM. Ovalbumin-specific CD45.1^{+} OT-II, tdtomato^{+} OT-II mice TCR transgenic, *CD4*^{Cre}*Rorc*$^{fl/wt}$ and *CD4*^{Cre}*Rorc*$^{fl/fl}$[73] were bred at EBM at the University of Gothenburg. We used both female and male mice which were eight to twelve weeks old in the experiments.

Sampling of human subjects

Written consents were obtained from the study participants before obtaining the samples. Ethical permit (ethical permit number: 2023-07055-01) was obtained by the Swedish Ethical Review Authority to collect venous blood and nasopharyngeal swabs from healthy subjects aged between 18-60 years old. Both male and female volunteers were included. We excluded the subjects who fulfilled any of the following criteria: respiratory infection during the last two weeks, allergic rhinitis, chronic obstructive pulmonary disease, asthma, regular nose bleeding, immunodeficiency and IAV infection in the last two years (verified by PCR).

Nearly 8 ml of venous blood was collected into lithium heparin coated tubes and was subjected to density gradient centrifugation to obtain peripheral blood mononuclear cells (PBMC) using lymphoprep (Stemcell Technnologies) according to manufacturer's instructions.

Nasopharyngeal cells (NT) were collected into 3 ml RPMI containing 2% fetal calf serum (FCS) and 1.5 mM DTT as previously described[19]. The cells were vortexed for 1 min and were incubated at 37°C for 30 min. The cells were spun at 700xg for 8 min at 4°C and the cell pellets were suspended in FACS buffer.

Infection of mice

Mouse adapted Influenza A/Puerto Rico/8/34 (PR8) (molecular clone; H1N1) and Influenza A/HK/x31 (HKx31)) (molecular clone; H3N2) were grown in 10 day old embryonated chicken eggs. The allantoic fluid was harvested and the viral titer was determined using $TCID_{50}$ assay. PR8 containing $Ova_{323-339}$ (PR8-Ova)[103] was kindly gifted by Paul G. Thomas, St. Jude Children's Research Hospital, USA. For sublethal total respiratory tract infection (TRT infection), mice were briefly anesthetized using isoflurane and inoculated intranasally with a sublethal dose (50 $TCID_{50}$) of mouse adapted Influenza A/Puerto Rico/8/34 (PR8) (Molecular

clone; H1N1) diluted in HBSS containing 0.1% BSA (total volume of 25 µl). For rechallenge experiment, a lethal dose of 5000 $TCID_{50}$ of X31 strain was used. To enhance the amount of CD4 TRM in the NT, mice were infected with a high dose (10^5 TCID50) of PR8 or PR8-Ova in a volume of 5 µl (URT restricted infection) 30 minutes after the TRT infection. The combined URT and TRT infection was performed for microscopy and single cell RNA sequencing.

Immunization of mice

5µg CTA1-3M2e-DD fusion protein was diluted in 1X PBS to an end volume of 5µl. BALB/c mice were immunized with CTA1-3M2e-DD intranasally and boosted twice with a ten-day interval. Control group was immunized with 5µg CTA1-DD adjuvant similarly.

Blocking of CXCL16 and depletion of T cells *in vivo*

Mouse CXCL16 antibody (MAB503) was purchased from R&D systems and was dissolved in 1X PBS. The antibody was administered intraperitoneally at a dosage of 2.5µg/g weight of mouse on day 1, 3, 6 and 9 post infection with PR8. Mice treated with equal amount of *InVivo*MAb rat IgG2a isotype control, anti-trinitrophenol (BE0089, Bioxcell) were used as controls.

*InVivo*MAb anti-mouse CD8α (BE0117), *InVivo*MAb anti-mouse CD4 (BE0003-1) and *InVivo*MAb rat IgG2b isotype control (BE0090) were purchased from Bioxcell and were administered intraperitoneally at a daily dosage of 10µg/g of mouse from day 28 to day 32 following PR8 infection.

Fingolimod treatment

10mg/ml stock of fingolimod (Cayman Chemicals) was prepared in DMSO. We administrated fingolimod at a dosage of 2.5 µg/g weight of mouse dissolved in sterile physiological saline solution by intraperitoneal injection at indicated days.

Adoptive transfer of antigen specific T cells

For adoptive transfer of OT-II$^+$ CD4 T cells, CD45.1$^+$ OT-II or tdtomato$^+$ OT-II mice were euthanized, and spleens were collected. Spleens were mashed and made into single cell suspension by passing through a 70µm strainer. Total CD4 T cells were isolated using EasySep mouse CD4+ T cell isolation kit (Stemcell technologies) according to manufacturer's instruction. A total of $5x10^6$ OT-II$^+$ CD4 T cells suspended in 1X PBS were administrated by intravenous injection four hours prior to infection with PR8-Ova.

For generation of effector OT-II T cells, we isolated CD4 T cells from splenocytes of tdtomato$^+$ OT-II mice. OT-II T cells were stimulated by culturing with splenocytes pulsed with 1uM Ova peptide ISQAVHAAHAEINEAGR in 5:1 ratio respectively in RPMI media containing 10% FBS, 10µg/ml gentamycin, 55µM β-mercaptoethanol (Gibco) and 20U/ml murine IL-2 (Peprotech) for 60h in 5% CO2 cell culture incubator. The cells were washed and incubated with fluorochrome conjugated antibodies against surface antigens- CD3 PerCPCy5.5 (17A2), CD4 APC-Cy7 (RM4-4) and CD69 BV605 (H1.2F3) for 20 min at 4°C. To exclude dead cells, the cells were washed and stained with LIVE/DEAD™ Fixable Aqua Dead Cell Stain (cat. no: L34957, Invitrogen) according to manufacturer's instruction. Cells were suspended in FACS buffer and live CD3$^+$CD4$^+$CD69$^-$ dtomato$^+$ OT-II effector T cells were collected after sorting in a BD FACSAria fusion (BD Biosciences). A total of $5x10^5$ effector OT-II$^+$ CD4 T cells

suspended in 1X PBS were administrated by intravenous injection two days post infection with PR8 or PR8-Ova.

Bone marrow chimera

For myeloablation, CD45.1^{+} B6.SJL-*Ptprc*^{a} *Pepc*^{b}/BoyJ mice were irradiated with 11 Gy in equally split doses with a 4-hour gap in a RS 2000 X ray irradiator machine. The mice were rested for a day and transplanted with a mix of 2.5 x 10^{6} tdtomato^{+} WT and 2.5 x 10^{6} CD45.2^{+} *Cxcr6*-/- bone marrow cells (BM) by intravenous administration. The recipients with newly reconstituted BM (BM chimera) were infected with 50 TCID50 PR8 intravenously 70 days after transplantation.

Isolation and processing of blood, lungs, NALT and nasal tissue

For flow cytometry experiments, mice were injected with CD4 FITC or CD4 APC-Cy7 (RM4-4) antibody intravenously to label the circulating CD4 T cells. The mice were completely anesthetized, and blood was withdrawn into EDTA coated tubes from the heart after five minutes of *in vivo* antibody labelling. The lung was perfused with 1X PBS and processed into single cell suspension using the mouse lung dissociation kit (Miltenyi Biotec). Blood was treated with RBC lysis buffer for five minutes, washed and resuspended in FACS buffer. Nasal tissue and NALT were isolated and processed immediately as previously described[14]. Nasal tissue was digested in 3 ml RPMI 1640 media supplemented with 2% FBS, 6 mg collagenase type 3 (Worthington Biochemical corporation) and 600 µg DNase I, grade II from bovine pancreas (Sigma Aldrich) in a shaking incubator at 37°C for one hour. The cells were made into single cell suspension by straining through a 70 µm nylon mesh. NALT was obtained by peeling the upper palate and the cells were extracted by teasing the NALT between two frosted slides. The cells were washed and resuspended in FACS buffer or supplemented media for downstream processing.

Stimulation of mouse cells with IAV peptides

The cells were stained for extracellular markers prior to stimulation with peptides. The following IAV peptide array were obtained from obtained from BEI resources, NIAID, NIH: Influenza Virus A/New York/348/2003 (H1N1) Nucleoprotein (NP) (NR-50714), A/New York/444/2001 (H1N1) Nonstructural protein 1 (NS1), Influenza Virus A/Puerto Rico/8/1934 (H1N1) Hemagglutinin (HA) (NR-18973) and Influenza Virus A/Puerto Rico/8/1934 (H1N1) Neuraminidase (NA) (NR-19257). 1µg each of all peptides from the peptide array are mixed to obtain the respective peptide pools.10 million cells derived from lungs and nasal tissue were stimulated with IAV NP, NS1, HA and NA peptide pools containing 1 µg of each peptide pool in RPMI 1640 supplemented with 10% FBS, 1% Penicillin/Streptomycin and Protein Transport Inhibitor (Containing Brefeldin A) (diluted 1:1000) (BD, 555029). The cells were incubated for four hours at 37°C and further washed with 1x PBS to proceed for intracellular cytokine staining.

Stimulation and flow cytometry of human PBMC and nasopharyngeal cells

PBMC and NT cells were incubated with Human Trustain FcX (Biolegend, 422302) for 10 min at 4°C. The cells were incubated with anti-human CD69 BV421 antibody (clone: FNXO) for 20 min at 4°C and washed with FACS buffer. The cells were resuspended in T cell stimulation media (RPMI 1640 supplemented with 10% FBS, 1% Penicillin/Streptomycin, Protein Transport Inhibitor (Containing Brefeldin A) (diluted 1:1000) (BD, 555029), Monensin

(Biolegend, 420701) and anti- human CD28/CD49d (BD, 347690)[104]. The cells were stimulated with peptide pools containing 2ug each of all peptides from Influenza Virus A/New York/348/2003 (H1N1) Nucleoprotein (NP) (NR-50714) peptide array and Influenza Virus A/New York/348/2003 (H1N1) Matrix protein 1 (M1) (NR-2613) peptide array for 6 hours at 37°C. Cells without the peptide pools were kept as unstimulated controls. After washing with FACS buffer, the cells were stained for extracellular antigens with the following fluorochrome conjugated antibodies (clone used indicated in bracket): anti-CD3 BUV737 (UCHT1), anti-CD4 PE-Dazzle594 (OKT4), anti-CD45RA BV605 (HI100), anti-CCR7 APC-Cy7 (G043H7), anti-CD103 FITC (Ber-ACT8) and anti-CXCR6 (13B1E5). After incubation at 4°C for 20 min, the cells were washed and stained with LIVE/DEAD™ Fixable Aqua Dead Cell Stain (cat. no: L34957, Invitrogen) according to manufacturer's instruction to exclude dead cells. To detect intracellular cytokines, the cells were fixed with 4% paraformaldehyde for 20 min at RT, washed with ice cold 1X PBS and permeabilized with permeabilization buffer (1XPBS containing 0.5% BSA and 0.5% saponin) for 10 min at RT. The cells were washed and resuspended in permeabilization buffer with the following fluorochrome conjugated antibody cocktail: anti- IFN-γ PE (25723.11), anti-TNF BV650 (MAb11) and anti-IL-17a APC (BL168). After incubation at 4°C overnight, the cells were washed and suspended in FACS buffer for data acquisition at BD LSR Fortessa X-20 or Sony spectral analyzer.

Flow cytometry of murine cells

All fluorochrome-conjugated antibodies are titrated to determine the optimal concentration for flow cytometry. Single cell suspension from organs were prepared and resuspended in FACS buffer as mentioned before. The following antibodies are used for mouse extracellular antigen staining: anti-CD3 PerCPCy5.5 (17A2), anti-CD4 FITC (RM4-4), anti-CD4 APC-Cy7 (RM4-5), anti-CD44 BV786 (IM7), anti-CD44 PE-Dazzle 594 (IM7), anti-CD62L BV711 (MEL-14), anti-CD69 BUV737 (H1.2F3), anti-CD11a PE-Cy7 (H155-78), anti-CD103 PE-Cy7 (2E7), anti-CD103 BV421 (2E7), anti-CD45.1 APC (A20), anti-CXCR6 BV421 (SA051D1), anti-ICOS BV421 (7E.17G9) and anti-PD1 PE (J43). The extracellular staining was performed by incubating the cells with the antibodies for 20 minutes at 4°C. For labelling antigen specific cells with tetramers, cells were incubated with fluorochrome labelled tetramers for 2h 40 min at 4°C and the extracellular antibody mix was added onto the top and incubated for 20 minutes. The following tetramers kindly provided by NIH tetramer core facility at Emory University were used: I-Ab $NP_{306-322}$ APC, I-A^d $M2e_{2-17}$ PE and I-Ab HA_{91-107} BV421. I-Ab human CLIP 87-101 conjugated with APC, PE or BV421 were used as negative controls. To exclude dead cells, the cells were washed and stained with LIVE/DEAD™ Fixable Aqua Dead Cell Stain (cat. no: L34957, Invitrogen) according to manufacturer's instruction. For intracellular cytokine staining, the cells were fixed with IC fixation buffer (eBioscience, 00-8222) for 60 minutes at room temparture. The cells were washed and resuspended in 1X permeabilization buffer (eBioscience, 00-8333) and incubated with the following antibodies: IL-2 BV785 (JES6-5H4), TNF BV421 (MP6-XT22), IFN-γ BV605 (XMG1.2) and IL-17a PE (TC11-18H10). The cells were washed with 1X permeabilization buffer and resuspended in FACS buffer. The labelled cells were run, and the data was acquired on the BD LSR Fortessa X-20 or BD LSR II (BD Biosciences) flow cytometer and was analyzed using Flow-Jo software (Tree Star).

Immunofluorescence staining

Mice were euthanized and upper part of mice heads were collected after removing the skin and eyeballs. The heads were fixed with 1.5% Formaldehyde Solution (w/v) (ThermoScientific)

solution at 4°C for 24 hours. After removing the teeth and remaining muscle tissues, they were transferred into 0.5M EDTA solution for decalcification for 7 days at 4°C. The samples were embedded into sequential dilutions of OCT paramount (Histolab) and were snap frozen for sectioning. 10-12 µm thick frontal sections thick sections were cut and SuperFrost microscopy slides. The slides were baked at 60°C for 1 hour and fixed with ice-cold acetone until the samples were dried. The tissue was blocked with 1X PBS containing 10% FBS and 5% Normal Rat Serum for 15 min at RT. After washing with 1X PBS, the tissues were stained with antibody cocktail containing anti-CD4 FITC (RM4-4) and anti-CD44 APC (IM7) overnight at 4°C in the dark. The sections were counterstained by incubating with Hoechst 33342 solution (Thermo) for 15 min at RT in the dark. The sections were mounted with a fluorescent mounting medium (Dako), acquired on an Axio Imager. Z2 (Zeiss) and analysed on TissueFACS Analyser (Version 7.1.120 Xylis).

TUNEL assay

Mice were euthanized and upper part of mice heads were collected after removing the skin and eyeballs. The heads were fixed with 4% Formaldehyde Solution (w/v) (ThermoScientific) solution at 4°C for 24 hours. After removing the teeth and remaining muscle tissues, they were transferred into 14% EDTA solution (w/v) for decalcification for 14 days at 4°C. The tissues were sequentially dehydrated and embedded into paraffin wax in a cassette. 4 µm thick sections were cut from the paraffinized tissue blocks. TUNEL assay kit -HRP-DAB (Abcam, ab206386) was used to detect apoptotic cells according to manufacturer´s instructions. The images were Axio Imager. Z2 (Zeiss) and analysed on TissueFACS Analyser (Version 7.1.120 Xylis) and QuPath (version 0.5.1) software.

Neutralization assay

200000 MDCK cells were plated in a 24 well plate and was incubated overnight at 37°C. Serum from IAV infected mice or mice immunized with irrelevant protein (streptavidin or SARSCoV2 spike protein) was serially diluted (two-fold) and incubated with 10^6 TCID50 X31 (MOI=5) in 500µl DMEM supplemented with 1mM HEPES, 1µg/ml TPCK trypsin and 5µg/ml gentamycin for 1 hour at 37°C. The plate containing MDCK cells was washed twice with 1x PBS and the virus/serum mixture was added onto the cells. The plate was incubated for 18 hours and washed twice with 1x PBS. The cells were incubated with 5x trypsin for cell detachment and the washed cells were fixed with fixation/permeabilization solution (eBioscience™ Foxp3 / Transcription Factor Staining Buffer Set, 00-5523-00) overnight at 4°C. The cells were washed twice with FACS buffer containing 0.1% saponin. The infected cells were labelled by incubating cells with InVivoMAb anti-Influenza A virus NP (clone H16-L10-4R5 (HB65)) (Bioxcell) labelled with alexa fluor 488 (Protein Labeling Kits for alexafluor 488, Invitrogen, A10235) for 30 minutes at 4°C. The cells were washed twice with FACS buffer containing 0.1% saponin and resuspended in FACS buffer for flow cytometry. The average signals from cells incubated with virus in the absence of serum was considered as 100% infectivity and is used to calculate the relative infectivity of cells in presence of serum.

Viral titer determination

Lung and URT (nasal tissue and NALT) are harvested and suspended in 1ml 1x PBS per 0.5g of organ. The tissues were homogenized using a tissue homogenizer and spun at 1200xg for 10 min at 4°C. The supernatant was used for determining the viral titer using the standard $TCID_{50}$ assay.

Single cell RNA sequencing

Mice were injected with CD4 FITC (RM4-4) antibody intravenously to label the circulating CD4 T cells (referred as CD4 iv). The mice were completely anesthetized and the lung was perfused with 1X PBS. Nasal tissue and lungs were isolated, digested and processed into single cells as described before. The samples were enriched for CD4 T cells using the EasySep™ mouse CD4+ T Cell isolation kit (Stemcell technologies) and the dead cells were removed using EasySep™ Dead Cell Removal (Annexin V) Kit (Stemcell technologies) according to manufacturer's instruction. Cells from PR8 infected mice were labelled with the following fluorochrome-conjugated MHC-II tetramers: I-Ab $NP_{306-322}$ APC and I-Ab HA_{91-107} BV421 as described before. After washing with FACS buffer, cells were labelled with TotalSeq™-C0987 anti-APC antibody (408007, Biolegend) to identify NP-specific CD4 TRM. Cells were washed and labelled with the antibodies. The following fluorochrome labelled antibodies were used: CD3 PerCPCy5.5 (17A2), CD4 APC-Cy7 (RM4-4) (for labelling tissue resident CD4 Tc- referred as CD4 tissue) and CD69 BV605 (H1.2F3) and CD44 PE-Dazzle 594 (IM7) and CD62L BV711 (MEL-14). Additionally, totalSeq-C0595 anti-mouse CD11a antibody (101131, Biolegend) and the following barcoded hashtag antibodies were used: hashtag antibodies 3,5-9 (155865, 155869, 155871, 155873, 155875, 15587; Biolegend) for demultiplexing of samples during data processing and to detect cells expressing CD11a protein on the cell surface. Live total CD4 TRM (CD4 iv^- CD4 $tissue^+CD44^+CD62L^-CD69^+$) were sorted from PR8 infected and naïve mice while NP-specific CD4 TRM ($NP_{306-322}^+$ CD4 iv^- CD4 $tissue^+CD44^+CD62L^-CD69^+$) and HA-specific CD4 TRM (HA_{91-107}^+ CD4 iv^- CD4 $tissue^+CD44^+CD62L^-CD69^+$) were sorted from PR8 infected mice. In addition to CD4 T cells, we sorted total live cells devoid of CD4 T cells from the NT of naïve and PR8 infected mice. The sorted cells were collected in a BD FACSAria fusion (BD Biosciences) cell sorter and processed immediately. The total number of cells sorted from each group are the following. Lung total CD4 TRM from naïve mice: 8000 cells, NT total CD4 TRM from naïve mice: 3095 cells, lung NP-specific CD4 TRM: 4002 cells, NT NP-specific CD4 TRM: 1172 cells, lung HA-specific CD4 TRM: 4073 cells, NT HA-specific CD4 TRM: 1314 cells, lung total CD4 TRM from infected mice: 8000 cells, NT total CD4 TRM from infected mice: 3000 cells, live cells except CD4 T cells from NT of naïve and infected mice: 10000 cells each. The sorted cells were pooled and washed in the Laminar Wash Mini system (Curiox Biosystems).

A maximum of 20,000 cells were processed into single cells in a chromium controller (10X Genomics). The single cell gene expression, TCR VDJ and cell surface protein (CSP) libraries were prepared using Chromium Next GEM Single Cell 5' Reagent Kits v2 (Dual Index) kit (PN-1000265), library construction kit (PN-1000190), 5' Feature Barcode Kit (PN-1000256), Chromium Single Cell Mouse TCR Amplification Kit (PN-1000254), Chromium Next GEM Chip K Single Cell Kit (1000286), Dual Index Kit TT Set A (PN-1000215) and Dual Index Kit TN Set A (PN-1000250). The prepared cDNA libraries were quantified using Qubit Fluorometer (Invitrogen) and quality was assessed using Agilent Tapestation system. The libraries were sequenced on Illumina NovaSeq 6000 by SNP&SEQ Technology Platform, Science for Life Laboratory (Uppsala Biomedical Centre, Uppsala University, Sweden) according to sequencing instructions provided by 10x Genomics.

Single cell RNA seq data processing

Raw fastq files were processed through the 10X cellranger pipeline using the multi command and default parameters with reference genome GRCm38-mm10. Raw UMI count matrices

generated from the cellranger 10X pipeline were loaded and merged into a single Seurat object (Seurat version 4)[105, 106, 107]. Cells were discarded if they met any of the following criteria: percentage of mitochondrial counts > 15%, number of unique features or total counts was in the bottom or top 0.5% of all cells, and number of unique features < 250. Gene counts were normalized to the same total counts per cell and were natural log transformed (after the addition of a pseudocount of 1). The normalized counts in each cell were mean-centered and scaled by their SD, and the following variables were regressed out: percentage of mitochondrial counts, percentage of ribosomal counts, G2M and S phase scores, TCR gene expression scores. Hashtags and APC-surface antibody were normalized by a centered log-ratio (CLR) normalization and binding assigned using HTODemux function. Data integration across cells originating from different samples was done using the Anchor method within Seurat. Selection of the number of components for the nearest-neighbor network computation was based on their visualization in an elbow plot. UMAP (65) was performed for the spatial visualization of the single-cell data set after features and cells were clustered using the Louvain algorithm. TCR data was processed using scRepertoire package[62] with standard setting. T cell clonality was based on identical nucleotide sequence in the CDR3 region. All TCR information were integrated with the scRNA-Seq data by aligning and merging the data with the metadata slot in the processed RNA-Seq Seurat object. Differentially expressed genes between different clusters were identified using the FindAllMarkers function from Seurat using default settings (Wilcoxon test and Bonferroni P value correction). Significant genes with average log fold change > 0.25 and expressed in > 25% of cells in that group were ranked according to fold change and are reported in supplementary table 1. For comparison between 2 groups, the FindMarkers function was used, and either top and bottom 20 genes were represented by Heatmap using the DoHeatmap function of Seurat or all genes were represented on a VolcanoPlot using the EnhancedVolcano R package[108]. Gene signatures were added to the Seurat object using the AddModuleScore function.

Statistical analysis

The data was analyzed using GraphPad prism software. The experiments were performed and analyzed in a non-blinded fashion. Both male and female mice were included in the experiments. For statistical analysis, unpaired two-tailed *t*test, one-way ANOVA, with Tukey's multiple comparison test, two-way ANOVA, Tukey's multiple comparison test or two-sided Wilcoxon matched-pairs signed-rank test and is indicated in the figure legends. Differences were considered significant when the P-value was <0.05. Outliers were identified and removed using Grubbs method (alpha=0.05) when indicated in the figure legend.

Data availability

Single-cell RNA-seq data have been deposited in the NCBI GEO database under accession number [xxx]. All other data are present in the article and Supplementary Information or are available from the corresponding author upon reasonable request.

References

1. Paget, J. *et al.* Global mortality associated with seasonal influenza epidemics: New burden estimates and predictors from the GLaMOR Project. *Journal of global health* **9**, 020421 (2019).

2. Campbell, A.P. *et al.* Vaccine Effectiveness Against Pediatric Influenza Hospitalizations and Emergency Visits. *Pediatrics* **146** (2020).

3. The, L. H5N1: international failures and uncomfortable truths. *Lancet (London, England)* **403**, 2455 (2024).

4. Vijayanand, S., Gomes, K.B., Gala, R.P., Uddin, M.N. & D'Souza, M.J. Exploring the Potential of T-Cells for a Universal Influenza Vaccine. *Vaccines* **8** (2020).

5. Marchesini Tovar, G., Gallen, C. & Bergsbaken, T. CD8+ Tissue-Resident Memory T Cells: Versatile Guardians of the Tissue. *Journal of immunology (Baltimore, Md. : 1950)* **212**, 361-368 (2024).

6. Zheng, M.Z.M. *et al.* Single-cycle influenza virus vaccine generates lung CD8(+) Trm that cross-react against viral variants and subvert virus escape mutants. *Science advances* **9**, eadg3469 (2023).

7. Teijaro, J.R. *et al.* Cutting edge: Tissue-retentive lung memory CD4 T cells mediate optimal protection to respiratory virus infection. *Journal of immunology (Baltimore, Md. : 1950)* **187**, 5510-5514 (2011).

8. Son, Y.M. *et al.* Tissue-resident CD4(+) T helper cells assist the development of protective respiratory B and CD8(+) T cell memory responses. *Science immunology* **6** (2021).

9. Swarnalekha, N. *et al.* T resident helper cells promote humoral responses in the lung. *Science immunology* **6** (2021).

10. Borkner, L., Curham, L.M., Wilk, M.M., Moran, B. & Mills, K.H.G. IL-17 mediates protective immunity against nasal infection with Bordetella pertussis by mobilizing neutrophils, especially Siglec-F(+) neutrophils. *Mucosal immunology* **14**, 1183-1202 (2021).

11. Brown, D.M., Lee, S., Garcia-Hernandez Mde, L. & Swain, S.L. Multifunctional CD4 cells expressing gamma interferon and perforin mediate protection against lethal influenza virus infection. *Journal of virology* **86**, 6792-6803 (2012).

12. Omokanye, A. *et al.* Clonotypic analysis of protective influenza M2e-specific lung resident Th17 memory cells reveals extensive functional diversity. *Mucosal immunology* **15**, 717-729 (2022).

13. Randall, T.D. *Structure, Organization, and Development of the Mucosal Immune System of the Respiratory Tract*. Mucosal Immunology. 2015:43-61. doi: 10.1016/B978-0-12-415847-4.00004-5. Epub 2015 Mar 13.

14. Pizzolla, A. *et al.* Resident memory CD8(+) T cells in the upper respiratory tract prevent pulmonary influenza virus infection. *Science immunology* **2** (2017).

15. Pizzolla, A. *et al.* Nasal-associated lymphoid tissues (NALTs) support the recall but not priming of influenza virus-specific cytotoxic T cells. *Proceedings of the National Academy of Sciences of the United States of America* **114**, 5225-5230 (2017).

16. Ziv Shulman, J.L., Liat Stoler-Barak, Hadas Hezroni-Bravyi, Adi Biram,Sacha Lebon, Natalia Davidzohn, Merav Kedmi, Muriel Chemla, David Pilzer, Marina Cohen, Ori Brenner, Moshe Biton. The origins of IgA-secreting cells in the acinar structures of the nasal turbinates. *Researchsquare* (2023).

17. Yount, K.S. *et al.* Systemic priming and intranasal booster with a BcfA-adjuvanted acellular pertussis vaccine generates CD4+ IL-17+ nasal tissue resident T cells and reduces B. pertussis nasal colonization. *Frontiers in immunology* **14**, 1181876 (2023).

18. O'Hara, J.M. *et al.* Generation of protective pneumococcal-specific nasal resident memory CD4(+) T cells via parenteral immunization. *Mucosal immunology* **13**, 172-182 (2020).

19. Lim, J.M.E. *et al.* SARS-CoV-2 breakthrough infection in vaccinees induces virus-specific nasal-resident CD8+ and CD4+ T cells of broad specificity. *The Journal of experimental medicine* **219** (2022).

20. Kinnear, E. *et al.* Airway T cells protect against RSV infection in the absence of antibody. *Mucosal immunology* **11**, 249-256 (2018).

21. Xu, Q. *et al.* Adaptive immune responses to SARS-CoV-2 persist in the pharyngeal lymphoid tissue of children. *Nature immunology* **24**, 186-199 (2023).

22. Diallo, B.K. *et al.* Intranasal COVID-19 vaccine induces respiratory memory T cells and protects K18-hACE mice against SARS-CoV-2 infection. *NPJ vaccines* **8**, 68 (2023).

23. Wimmers, F. *et al.* Multi-omics analysis of mucosal and systemic immunity to SARS-CoV-2 after birth. *Cell* **186**, 4632-4651.e4623 (2023).

24. Richard, M. *et al.* Influenza A viruses are transmitted via the air from the nasal respiratory epithelium of ferrets. *Nature communications* **11**, 766 (2020).

25. Uddbäck, I. *et al.* Prevention of respiratory virus transmission by resident memory CD8(+) T cells. *Nature* **626**, 392-400 (2024).

26. Shiow, L.R. *et al.* CD69 acts downstream of interferon-alpha/beta to inhibit S1P1 and lymphocyte egress from lymphoid organs. *Nature* **440**, 540-544 (2006).

27. Szabo, P.A., Miron, M. & Farber, D.L. Location, location, location: Tissue resident memory T cells in mice and humans. *Science immunology* **4** (2019).

28. Zens, K.D. *et al.* Reduced generation of lung tissue-resident memory T cells during infancy. *The Journal of experimental medicine* **214**, 2915-2932 (2017).

29. Beura, L.K. *et al.* CD4(+) resident memory T cells dominate immunosurveillance and orchestrate local recall responses. *The Journal of experimental medicine* **216**, 1214-1229 (2019).

30. Miller, M.A., Ganesan, A.P., Luckashenak, N., Mendonca, M. & Eisenlohr, L.C. Endogenous antigen processing drives the primary CD4+ T cell response to influenza. *Nature medicine* **21**, 1216-1222 (2015).

31. Turner, D.L. *et al.* Lung niches for the generation and maintenance of tissue-resident memory T cells. *Mucosal immunology* **7**, 501-510 (2014).

32. Brinkmann, V. *et al.* The immune modulator FTY720 targets sphingosine 1-phosphate receptors. *The Journal of biological chemistry* **277**, 21453-21457 (2002).

33. Eliasson, D.G. *et al.* CTA1-M2e-DD: a novel mucosal adjuvant targeted influenza vaccine. *Vaccine* **26**, 1243-1252 (2008).

34. Eliasson, D.G. *et al.* M2e-tetramer-specific memory CD4 T cells are broadly protective against influenza infection. *Mucosal immunology* **11**, 273-289 (2018).

35. Takamura, S. *et al.* Specific niches for lung-resident memory CD8+ T cells at the site of tissue regeneration enable CD69-independent maintenance. *The Journal of experimental medicine* **213**, 3057-3073 (2016).

36. Künzli, M. & Masopust, D. CD4(+) T cell memory. *Nature immunology* **24**, 903-914 (2023).

37. Wang, Z. *et al.* PD-1(hi) CD8(+) resident memory T cells balance immunity and fibrotic sequelae. *Science immunology* **4** (2019).

38. Moguche, A.O. *et al.* ICOS and Bcl6-dependent pathways maintain a CD4 T cell population with memory-like properties during tuberculosis. *The Journal of experimental medicine* **212**, 715-728 (2015).

39. Peng, C. *et al.* Engagement of the costimulatory molecule ICOS in tissues promotes establishment of CD8(+) tissue-resident memory T cells. *Immunity* **55**, 98-114.e115 (2022).

40. Andreatta, M. *et al.* A CD4(+) T cell reference map delineates subtype-specific adaptation during acute and chronic viral infections. *eLife* **11** (2022).

41. Hashimoto, K. *et al.* Single-cell transcriptomics reveals expansion of cytotoxic CD4 T cells in supercentenarians. *Proceedings of the National Academy of Sciences of the United States of America* **116**, 24242-24251 (2019).

42. Woodring, T. *et al.* Distinctive populations of CD4(+)T cells associated with vaccine efficacy. *iScience* **25**, 104934 (2022).

43. Kurd, N.S. *et al.* Early precursors and molecular determinants of tissue-resident memory CD8(+) T lymphocytes revealed by single-cell RNA sequencing. *Science immunology* **5** (2020).

44. Dey, S. *et al.* Downregulation of MALAT1 is a hallmark of tissue and peripheral proliferative T cells in COVID-19. *Clinical and experimental immunology* **212**, 262-275 (2023).

45. Plasek, L.M. & Valadkhan, S. lncRNAs in T lymphocytes: RNA regulation at the heart of the immune response. *American journal of physiology. Cell physiology* **320**, C415-c427 (2021).

46. Wang, X. *et al.* Reinvestigation of Classic T Cell Subsets and Identification of Novel Cell Subpopulations by Single-Cell RNA Sequencing. *Journal of immunology (Baltimore, Md. : 1950)* **208**, 396-406 (2022).

47. Yang, H.Q., Wang, Y.S., Zhai, K. & Tong, Z.H. Single-Cell TCR Sequencing Reveals the Dynamics of T Cell Repertoire Profiling During Pneumocystis Infection. *Frontiers in microbiology* **12**, 637500 (2021).

48. Li, J., Lu, E., Yi, T. & Cyster, J.G. EBI2 augments Tfh cell fate by promoting interaction with IL-2-quenching dendritic cells. *Nature* **533**, 110-114 (2016).

49. Yan, Y. *et al.* TCR stimulation upregulates MS4a4B expression through induction of AP-1 transcription factor during T cell activation. *Molecular immunology* **52**, 71-78 (2012).

50. Cohen, N.R. *et al.* Shared and distinct transcriptional programs underlie the hybrid nature of iNKT cells. *Nature immunology* **14**, 90-99 (2013).

51. Hu, X. *et al.* Single-cell transcriptomics reveals distinct cell response between acute and chronic pulmonary infection of Pseudomonas aeruginosa. *MedComm* **3**, e193 (2022).

52. Tuomela, K., Ambrose, A.R. & Davis, D.M. Escaping Death: How Cancer Cells and Infected Cells Resist Cell-Mediated Cytotoxicity. *Frontiers in immunology* **13**, 867098 (2022).

53. Ng, S.S. *et al.* Author Correction: The NK cell granule protein NKG7 regulates cytotoxic granule exocytosis and inflammation. *Nature immunology* **25**, 716 (2024).

54. Szabo, P.A. *et al.* Single-cell transcriptomics of human T cells reveals tissue and activation signatures in health and disease. *Nature communications* **10**, 4706 (2019).

55. Hoft, S.G. *et al.* The Rate of CD4 T Cell Entry into the Lungs during Mycobacterium tuberculosis Infection Is Determined by Partial and Opposing Effects of Multiple Chemokine Receptors. *Infection and immunity* **87** (2019).

56. Brownlie, D. *et al.* Comparison of Lung-Homing Receptor Expression and Activation Profiles on NK Cell and T Cell Subsets in COVID-19 and Influenza. *Frontiers in immunology* **13**, 834862 (2022).

57. Rauen, T., Hedrich, C.M., Tenbrock, K. & Tsokos, G.C. cAMP responsive element modulator: a critical regulator of cytokine production. *Trends in molecular medicine* **19**, 262-269 (2013).

58. Devaiah, B.N. *et al.* Novel functions for TAF7, a regulator of TAF1-independent transcription. *The Journal of biological chemistry* **285**, 38772-38780 (2010).

59. Nguyen, K.D. *et al.* XCL1 enhances regulatory activities of CD4+ CD25(high) CD127(low/-) T cells in human allergic asthma. *Journal of immunology (Baltimore, Md. : 1950)* **181**, 5386-5395 (2008).

60. Mas-Orea, X. *et al.* Proenkephalin deletion in hematopoietic cells induces intestinal barrier failure resulting in clinical feature similarities with irritable bowel syndrome in mice. *Communications biology* **6**, 1168 (2023).

61. Kourepini, E. *et al.* Osteopontin expression by CD103- dendritic cells drives intestinal inflammation. *Proceedings of the National Academy of Sciences of the United States of America* **111**, E856-865 (2014).

62. Borcherding, N., Bormann, N.L. & Kraus, G. scRepertoire: An R-based toolkit for single-cell immune receptor analysis. *F1000Research* **9**, 47 (2020).

63. Mabrouk, N. *et al.* CXCR6 expressing T cells: Functions and role in the control of tumors. *Frontiers in immunology* **13**, 1022136 (2022).

64. Wein, A.N. *et al.* CXCR6 regulates localization of tissue-resident memory CD8 T cells to the airways. *The Journal of experimental medicine* **216**, 2748-2762 (2019).

65. Koenen, A. *et al.* The DRF motif of CXCR6 as chemokine receptor adaptation to adhesion. *PloS one* **12**, e0173486 (2017).

66. Wilbanks, A. *et al.* Expression cloning of the STRL33/BONZO/TYMSTRligand reveals elements of CC, CXC, and CX3C chemokines. *Journal of immunology (Baltimore, Md. : 1950)* **166**, 5145-5154 (2001).

67. Bodewes, R. *et al.* Prevalence of antibodies against seasonal influenza A and B viruses in children in Netherlands. *Clinical and vaccine immunology : CVI* **18**, 469-476 (2011).

68. Thome, J.J. *et al.* Spatial map of human T cell compartmentalization and maintenance over decades of life. *Cell* **159**, 814-828 (2014).

69. Jaffar, Z., Ferrini, M.E., Herritt, L.A. & Roberts, K. Cutting edge: lung mucosal Th17-mediated responses induce polymeric Ig receptor expression by the airway epithelium and elevate secretory IgA levels. *Journal of immunology (Baltimore, Md. : 1950)* **182**, 4507-4511 (2009).

70. Laan, M. *et al.* Neutrophil recruitment by human IL-17 via C-X-C chemokine release in the airways. *Journal of immunology (Baltimore, Md. : 1950)* **162**, 2347-2352 (1999).

71. Wang, X. *et al.* A critical role of IL-17 in modulating the B-cell response during H5N1 influenza virus infection. *Cellular & molecular immunology* **8**, 462-468 (2011).

72. Maroof, A., Yorgensen, Y.M., Li, Y. & Evans, J.T. Intranasal vaccination promotes detrimental Th17-mediated immunity against influenza infection. *PLoS pathogens* **10**, e1003875 (2014).

73. Gribonika, I. *et al.* Peyer's patch T(H)17 cells are dispensable for gut IgA responses to oral immunization. *Science immunology* **7**, eabc5500 (2022).

74. Ivanov, II *et al.* The orphan nuclear receptor RORgammat directs the differentiation program of proinflammatory IL-17+ T helper cells. *Cell* **126**, 1121-1133 (2006).

75. Dutta, A. *et al.* An IL-17-EGFR-TRAF4 axis contributes to the alleviation of lung inflammation in severe influenza. *Communications biology* **6**, 600 (2023).

76. Konieczny, P. *et al.* Interleukin-17 governs hypoxic adaptation of injured epithelium. *Science (New York, N.Y.)* **377**, eabg9302 (2022).

77. Bates, J.T. Naïve CD4(+) T Cell Activation in the Nasal-Associated Lymphoid Tissue following Intranasal Immunization with a Flagellin-Based Subunit Vaccine. *International journal of molecular sciences* **23** (2022).

78. Khan, T.N., Mooster, J.L., Kilgore, A.M., Osborn, J.F. & Nolz, J.C. Local antigen in nonlymphoid tissue promotes resident memory CD8+ T cell formation during viral infection. *The Journal of experimental medicine* **213**, 951-966 (2016).

79. McMaster, S.R. *et al.* Pulmonary antigen encounter regulates the establishment of tissue-resident CD8 memory T cells in the lung airways and parenchyma. *Mucosal immunology* **11**, 1071-1078 (2018).

80. Wakim, L.M., Woodward-Davis, A. & Bevan, M.J. Memory T cells persisting within the brain after local infection show functional adaptations to their tissue of residence. *Proceedings of the National Academy of Sciences of the United States of America* **107**, 17872-17879 (2010).

81. Zens, K.D., Chen, J.K. & Farber, D.L. Vaccine-generated lung tissue-resident memory T cells provide heterosubtypic protection to influenza infection. *JCI insight* **1** (2016).

82. Sato, A. *et al.* Vaginal memory T cells induced by intranasal vaccination are critical for protective T cell recruitment and prevention of genital HSV-2 disease. *Journal of virology* **88**, 13699-13708 (2014).

83. Bergsbaken, T. & Bevan, M.J. Proinflammatory microenvironments within the intestine regulate the differentiation of tissue-resident $CD8^+$ T cells responding to infection. *Nature immunology* **16**, 406-414 (2015).

84. Caminschi, I., Lahoud, M.H., Pizzolla, A. & Wakim, L.M. Zymosan by-passes the requirement for pulmonary antigen encounter in lung tissue-resident memory CD8(+) T cell development. *Mucosal immunology* **12**, 403-412 (2019).

85. Di Pilato, M. *et al.* CXCR6 positions cytotoxic T cells to receive critical survival signals in the tumor microenvironment. *Cell* **184**, 4512-4530.e4522 (2021).

86. Ashhurst, A.S. *et al.* CXCR6-Deficiency Improves the Control of Pulmonary Mycobacterium tuberculosis and Influenza Infection Independent of T-Lymphocyte Recruitment to the Lungs. *Frontiers in immunology* **10**, 339 (2019).

87. Kazer, S.W. *et al.* Primary nasal influenza infection rewires the tissue-scale memory response dynamics. *Immunity* (2024).

88. Fong, C.H. *et al.* Interferon-gamma inhibits influenza A virus cellular attachment by reducing sialic acid cluster size. *iScience* **25**, 104037 (2022).

89. Brass, A.L. *et al.* The IFITM proteins mediate cellular resistance to influenza A H1N1 virus, West Nile virus, and dengue virus. *Cell* **139**, 1243-1254 (2009).

90. Weiss, I.D. *et al.* IFN-gamma treatment at early stages of influenza virus infection protects mice from death in a NK cell-dependent manner. *Journal of interferon & cytokine research : the official journal of the International Society for Interferon and Cytokine Research* **30**, 439-449 (2010).

91. Feeley, E.M. *et al.* IFITM3 inhibits influenza A virus infection by preventing cytosolic entry. *PLoS pathogens* **7**, e1002337 (2011).

92. McKinstry, K.K. *et al.* Memory CD4+ T cells protect against influenza through multiple synergizing mechanisms. *The Journal of clinical investigation* **122**, 2847-2856 (2012).

93. Pandiyan, P. *et al.* Microbiome Dependent Regulation of T(regs) and Th17 Cells in Mucosa. *Frontiers in immunology* **10**, 426 (2019).

94. Brockmann, L. *et al.* Intestinal microbiota-specific Th17 cells possess regulatory properties and suppress effector T cells via c-MAF and IL-10. *Immunity* **56**, 2719-2735.e2717 (2023).

95. McCarthy, K.N., Hone, S., McLoughlin, R.M. & Mills, K.H.G. IL-17 and IFN-γ-producing respiratory tissue resident memory CD4 T cells persist for decades in adults immunized as children with whole cell pertussis vaccines. *The Journal of infectious diseases* (2024).

96. Lin, Y. *et al.* Interleukin-17 is required for T helper 1 cell immunity and host resistance to the intracellular pathogen Francisella tularensis. *Immunity* **31**, 799-810 (2009).

97. Mills, K.H.G. IL-17 and IL-17-producing cells in protection versus pathology. *Nature reviews. Immunology* **23**, 38-54 (2023).

98. Solans, L. *et al.* IL-17-dependent SIgA-mediated protection against nasal Bordetella pertussis infection by live attenuated BPZE1 vaccine. *Mucosal immunology* **11**, 1753-1762 (2018).

99. Liang, S.C. *et al.* Interleukin (IL)-22 and IL-17 are coexpressed by Th17 cells and cooperatively enhance expression of antimicrobial peptides. *The Journal of experimental medicine* **203**, 2271-2279 (2006).

100. Sonnenberg, G.F. *et al.* Pathological versus protective functions of IL-22 in airway inflammation are regulated by IL-17A. *The Journal of experimental medicine* **207**, 1293-1305 (2010).

101. Yang, N. *et al.* The 2009 pandemic A/Wenshan/01/2009 H1N1 induces apoptotic cell death in human airway epithelial cells. *Journal of molecular cell biology* **3**, 221-229 (2011).

102. Diallo, B.K. *et al.* Intranasal COVID-19 vaccine induces respiratory memory T cells and protects K18-hACE mice against SARS-CoV-2 infection. *NPJ vaccines* **8**, 68 (2023).

103. Thomas, P.G. *et al.* An unexpected antibody response to an engineered influenza virus modifies CD8+ T cell responses. *Proceedings of the National Academy of Sciences of the United States of America* **103**, 2764-2769 (2006).

104. Sekine, T. *et al.* Robust T Cell Immunity in Convalescent Individuals with Asymptomatic or Mild COVID-19. *Cell* **183**, 158-168.e114 (2020).

105. Satija, R., Farrell, J.A., Gennert, D., Schier, A.F. & Regev, A. Spatial reconstruction of single-cell gene expression data. *Nature biotechnology* **33**, 495-502 (2015).

106. Hao, Y. *et al.* Dictionary learning for integrative, multimodal and scalable single-cell analysis. *Nature biotechnology* **42**, 293-304 (2024).

107. Hao, Y. *et al.* Integrated analysis of multimodal single-cell data. *Cell* **184**, 3573-3587.e3529 (2021).

108. Blighe K, R.S., Lewis M EnhancedVolcano: Publication-ready volcano plots with enhanced colouring and labeling, R package version 1.22.0,https://github.com/kevinblighe/EnhancedVolcano. (2024).

Acknowledgments:

We would like to thank the staff at the Experimental Biomedicine (EBM) core facility at the University of Gothenburg for animal management; Paul G. Thomas, St. Jude Children's hospital for PR8-OVA virus; Linda M Wakim, Doherty Institute for providing protocol for processing of nasal tissue; Carina Karlsson, University of Gothenburg for providing access to microtome; Alvar Almstedt, Bioinformatics and Data Centre (BDC), Core Facilities, University of Gothenburg, for data pre-processing; Genomics core facility at Sahlgrenska Hospital for providing access to Qubit fluorometer and tapestation and study participants for providing samples. MHC-II tetramers were obtained from the NIH tetramer core facility. The following reagents were obtained through BEI Resources, NIAID, NIH: Peptide Array, Influenza Virus A/New York/348/2003 (H1N1) Nucleocapsid Protein, NR-50714 and Peptide Array, Influenza Virus A/New York/348/2003 (H1N1) Matrix protein 1 (M1) (NR-2613). Sequencing was performed by the SNP&SEQ Technology Platform in Uppsala. The facility is part of the National Genomics Infrastructure (NGI) Sweden and Science for Life Laboratory. The SNP&SEQ Platform is also supported by the Swedish Research Council and the Knut and Alice Wallenberg Foundation. The experiment schemes are created with Biorender.com.

Funding:

The project was supported by grants from the European Research Council (ERC-StG, B-DOMINANCE, grant no. 850638 to DA); the Swedish Research Council (grant no. 2021-01164, 2021-01165 to DA); the Knut and Alice Wallenberg Foundation (grant no 2021.0033 to DA) and the Sahlgrenska Academy (GU2020/2376-JNR2020 to DA). NRM is supported by Svenska Sällskapet för Medicinsk Forskning post-doctoral grant (grant no: PD20-0017), Elisabeth Bollan Linden stipend, Stiftelsen Lars Hiertas Minne and Stiftelsen Wilhelm och Martina Lundgrens Vetenskapsfond. KT is supported by grants from Svenska Sällskapet för Medicinsk Forskning (S21-0083).

Author contributions:

Conceptualization: NRM, DA. Methodology: NRM, RG, LS, KS, AS, MB, KT, DA. Formal analysis: NRM, RG, LS, KS, AS, NL, MB, KT, DA. Investigation: NRM, RG, LS, KS, MB, KT, DA. Data curation: DA, NRM. Software: DA, NRM. Resources: NL, MB. Project Administration: NRM, DA. Supervision: MB, NL, KT, DA. Funding Acquisition: DA, NRM. Writing – original draft: NRM, DA. Writing – review & editing: NRM, RG, LS, KS, AS, MB, KT, DA.

Competing interests:

The authors have no conflicts of interest to disclose.

Figures:

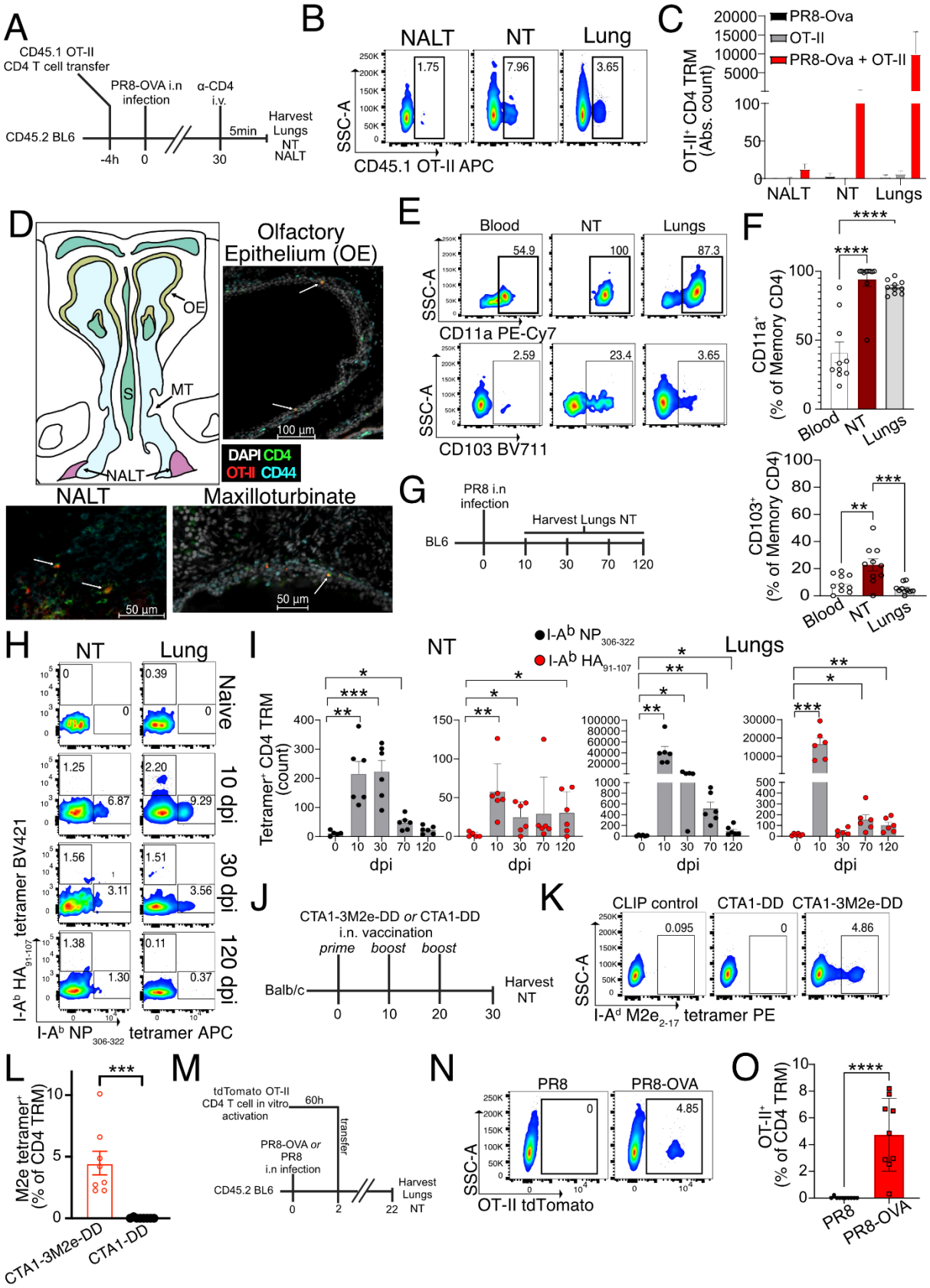
A
CD45.1 OT-II
CD4 T cell transfer
PR8-OVA i.n
infection
α-CD4
i.v.
CD45.2 BL6
-4h
0
30
5min
Harvest
Lungs
NT
NALT
B
NALT
NT
Lung
1.75
7.96
3.65
SSC-A
CD45.1 OT-II APC
C
PR8-Ova
OT-II
PR8-Ova + OT-II
OT-II+ CD4 TRM
(Abs. count)
NALT
NT
Lungs
D
Olfactory
Epithelium (OE)
OE
S
MT
NALT
100 µm
DAPI CD4
OT-II CD44
NALT
Maxilloturbinate
50 µm
50 µm
E
Blood
NT
Lungs
54.9
100
87.3
CD11a PE-Cy7
2.59
23.4
3.65
CD103 BV711
F
CD11a+
(% of Memory CD4)
Blood
NT
Lungs
CD103+
(% of Memory CD4)
G
PR8 i.n
infection
Harvest Lungs NT
BL6
0
10
30
70
120
H
NT
Lung
Naive
10 dpi
30 dpi
120 dpi
tetramer BV421
I-Ab HA91-107
I-Ab NP306-322 tetramer APC
I
I-Ab NP306-322
I-Ab HA91-107
NT
Lungs
Tetramer+ CD4 TRM
(count)
dpi
J
CTA1-3M2e-DD or CTA1-DD
i.n. vaccination
prime
boost
boost
Balb/c
Harvest
NT
K
CLIP control
CTA1-DD
CTA1-3M2e-DD
0.095
0
4.86
SSC-A
I-Ad M2e2-17 tetramer PE
L
M2e tetramer+
(% of CD4 TRM)
CTA1-3M2e-DD
CTA1-DD
M
tdTomato OT-II
CD4 T cell in vitro
activation
60h
transfer
PR8-OVA or
PR8
i.n infection
CD45.2 BL6
Harvest
Lungs
NT
N
PR8
PR8-OVA
0
4.85
SSC-A
OT-II tdTomato
O
OT-II+
(% of CD4 TRM)
PR8
PR8-OVA

Fig 1: IAV-specific CD4 TRM are formed at the URT and is dependent on presence of cognate antigen

A) Schematic diagram for the procedure of transfer of Ova specific (OT-II) CD4 T cells, infection of mice with PR8-Ova and subsequent harvesting of organs.

B-C) CD45.1$^+$ OT-II CD4 TRM in different organs of CD45.2$^+$ recipients on day 30 following PR8-Ova infection. B) Representative flow cytometry plots indicating the percentages of CD45.1$^+$ OT-II CD4 TRM. The data are representative of one experiment out of three independent experiments. C) Bar graph indicating the absolute number of CD45.1$^+$ or tomato$^+$ OT-II CD4 TRM. The experiment was repeated thrice and the results (mean ± s.e.m.) were pooled.

D) Representative microscopic images of OT-II$^+$ (red) CD4$^+$ (green) CD44$^+$ (cyan) T cells in different sections of the NT and NALT. The sections are derived from day 30 following PR8 Ova infection of mice that received OT-II CD4 T cells as described in fig. 1 A. Scale bars are indicated in each image.

E-F) Frequency of CD103$^+$ and CD11a$^+$ cells among OT-II CD4 TRM in NT and lungs, and among total CD4 effector memory T cells in blood of CD45.2$^+$ recipients on day 30 following IAV infection. E) Representative flow cytometry plots indicating the percentages of CD103$^+$ and CD11a$^+$ cells. The data is representative of one experiment out of two independent experiments. F) Scatter plot indicating the percentages of CD103$^+$ and CD11a$^+$ cells. Each data point indicates an individual mouse. The experiment was repeated twice and the results (mean ± s.e.m.) were pooled. NS, not significant, ****P<0.0001; ***P<0.001; **P<0.01; *P<0.05 by one-way ANOVA, with Tukey's multiple comparison test.

G-I) Kinetics of I-A^b NP$_{306-322}$ tetramer and I-A^b HA$_{91-107}$ tetramer- specific CD4 TRM in the NT and lungs on indicated days following PR8 IAV infection. G) Schematic representation of the experimental setup. H) Representative flow cytometry plots indicating the percentages of I-A^b NP$_{306-322}$ tetramer and I-A^b HA$_{91-107}$ tetramer- specific CD4 TRM are shown. I) Scatter plot indicating the absolute numbers of I-A^b NP$_{306-322}$ tetramer and I-A^b HA$_{91-107}$ tetramer- specific CD4 TRM. Each data point indicates an individual mouse. The experiment was performed once and the results (mean ± s.e.m.) were plotted. NS, not significant, ****P<0.0001; ***P<0.001; **P<0.01; *P<0.05 by unpaired two-tailed t-test.

J-L) I-A^d M2e$_{2-17}$ tetramer$^+$ CD4 TRM in the NT of BALB/c on day 30 post immunization with CTA1-DD or CTA1-3M2e-DD intranasally. J) Schematic representation of the experimental setup. K) Representative flow cytometry plots indicating the percentage of I-A^d M2e$_{2-17}$ tetramer$^+$ CD4 TRM from different treatment groups. Staining with I-A^d Human CLIP$_{87-101}$ tetramer (CLIP control) is used as the negative control. L) Scatter plot indicating the percentage of I-A^d M2e$_{2-17}$ tetramer$^+$ cells among all CD4 TRM. The experiment was repeated twice and the results (mean ± s.e.m.) were pooled. NS, not significant, ****P<0.0001; ***P<0.001; **P<0.01; *P<0.05 by unpaired two-tailed t-test.

M-O) Frequency of OT-II CD4 TRM in the NT on day 22 following infection with PR8 or PR8-Ova. M) Schematic representation of the experimental setup. N) A representative flow cytometry plot indicating the frequency of OT-II CD4 TRM. O) Scatter plot showing the frequency of OT-II CD4 TRM. The experiment was performed twice and

the results (mean ± s.e.m.) are pooled. NS, not significant, ****P<0.0001; ***P<0.001; **P<0.01; *P<0.05 by unpaired two-tailed t-test.

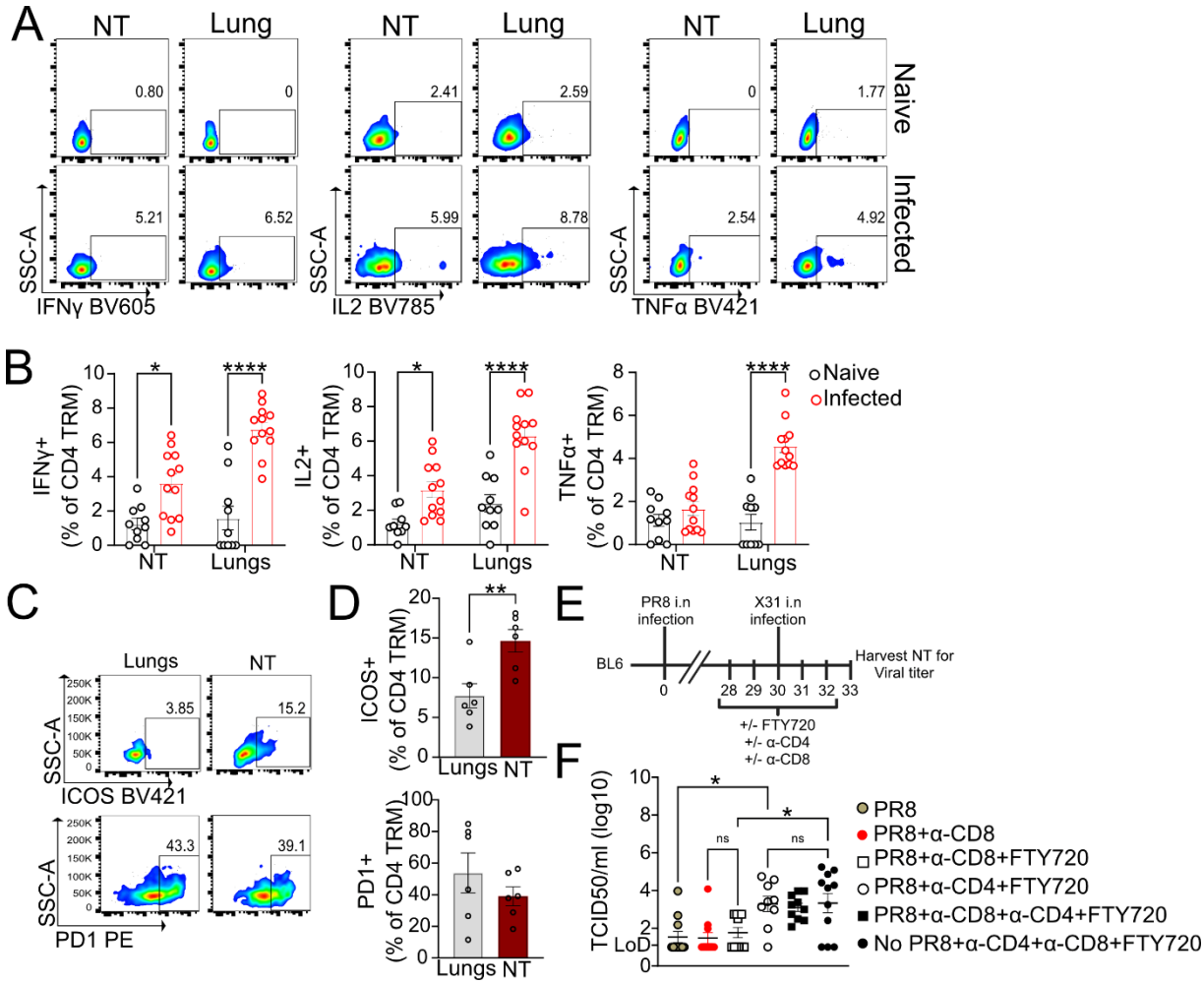

Fig 2: NT CD4 TRM are multifunctional and are indispensable for local viral clearance

A-B) Expression of intracellular cytokines in CD4 TRM of NT and lungs upon restimulation with IAV NP peptide pool. The organs are isolated on day 30 following PR8 IAV infection of mice or from naïve mice. A) Flow cytometry plots indicating the percentage of CD4 TRM expressing IFN-γ, IL-2 and TNF. B) Scatter plot showing the percentage of CD4 TRM expressing IFN-γ, IL-2 and TNF. The experiment was repeated thrice and the results (mean ± s.e.m.) are pooled. NS, not significant, ****P<0.0001; ***P<0.001; **P<0.01; *P<0.05 by two-way ANOVA, with Tukey's multiple comparison test.

C-D) Expression of ICOS and PD-1 on CD4 TRM on d30 post PR8 IAV infection. C) Representative flow cytometry plots of CD4 TRM expressing ICOS and PD-1 in lungs and NT. D) Scatter plot showing the percentage of CD4 TRM expressing ICOS and PD-1. The experiment was repeated twice and the results (mean ± s.e.m.) are pooled. NS, not significant, ****P<0.0001; ***P<0.001; **P<0.01; *P<0.05 by unpaired two-tailed t-test.

E) Schematic representation of primary and secondary infection of mice, their treatment with anti-CD4 antibody, anti-CD8 antibody or/and FTY720 on the indicated days and collection of NT.

F) Scatter plot indicating viral titers (TCID50/ml) in NT of mice on day 3 following secondary infection with X31 IAV. The experiment was repeated thrice and the results (mean ± s.e.m.) are pooled. NS, not significant, ****$P<0.0001$; ***$P<0.001$; **$P<0.01$; *$P<0.05$ by one-way ANOVA, with Tukey's multiple comparison test. The outliers were identified and removed using Grubbs method (alpha=0.05). One outlier each removed from all groups except for groups: PR8 + anti-CD8 + FTY720 and PR8 + anti-CD4.

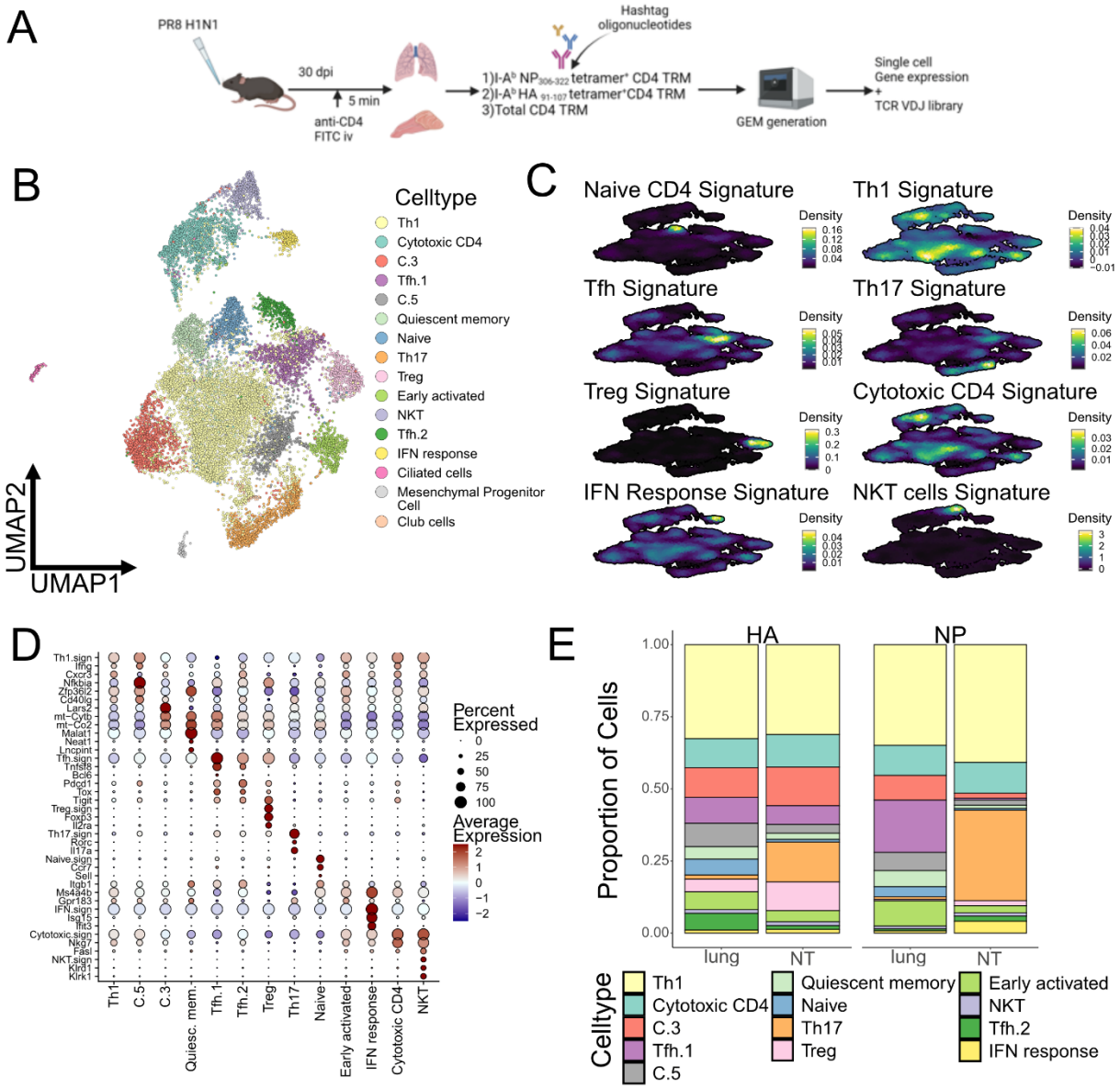

Fig 3: Single cell RNA sequencing of CD4 TRM delineates differential distribution of clusters between organs

A) Schematic diagram showing the preparation of antigen specific cells from PR8 IAV infected mice for generation of GEM using 10X Chromium controller.

B) UMAP plot of unsupervised clustering for 15301 CD4 TRM isolated from lungs and NT of naïve and PR8 IAV infected mice.

C) Density plot showing the expression of selected gene signatures, projected on the same UMAP as in B. Naïve CD4 T signature[46], Th1 signature[40], Tfh signature[40], Th17 signature[54], Treg signature[47], Cytotoxic CD4 signature[41], IFN response signature[54], NKT cells signature[50, 51].

D) Dot plot representing mean expression of selected marker genes for each T cell cluster. Color intensity from blue to red indicates average expression of genes and size of the dot depicts percentage of cells expressing the gene within the clusters. Only T cell clusters were included in the analysis.

E) Bar graph showing proportion of each UMAP cluster divided by organ and antigen specificity. Only antigen specific CD4 TRM from infected mice were included in the analysis.

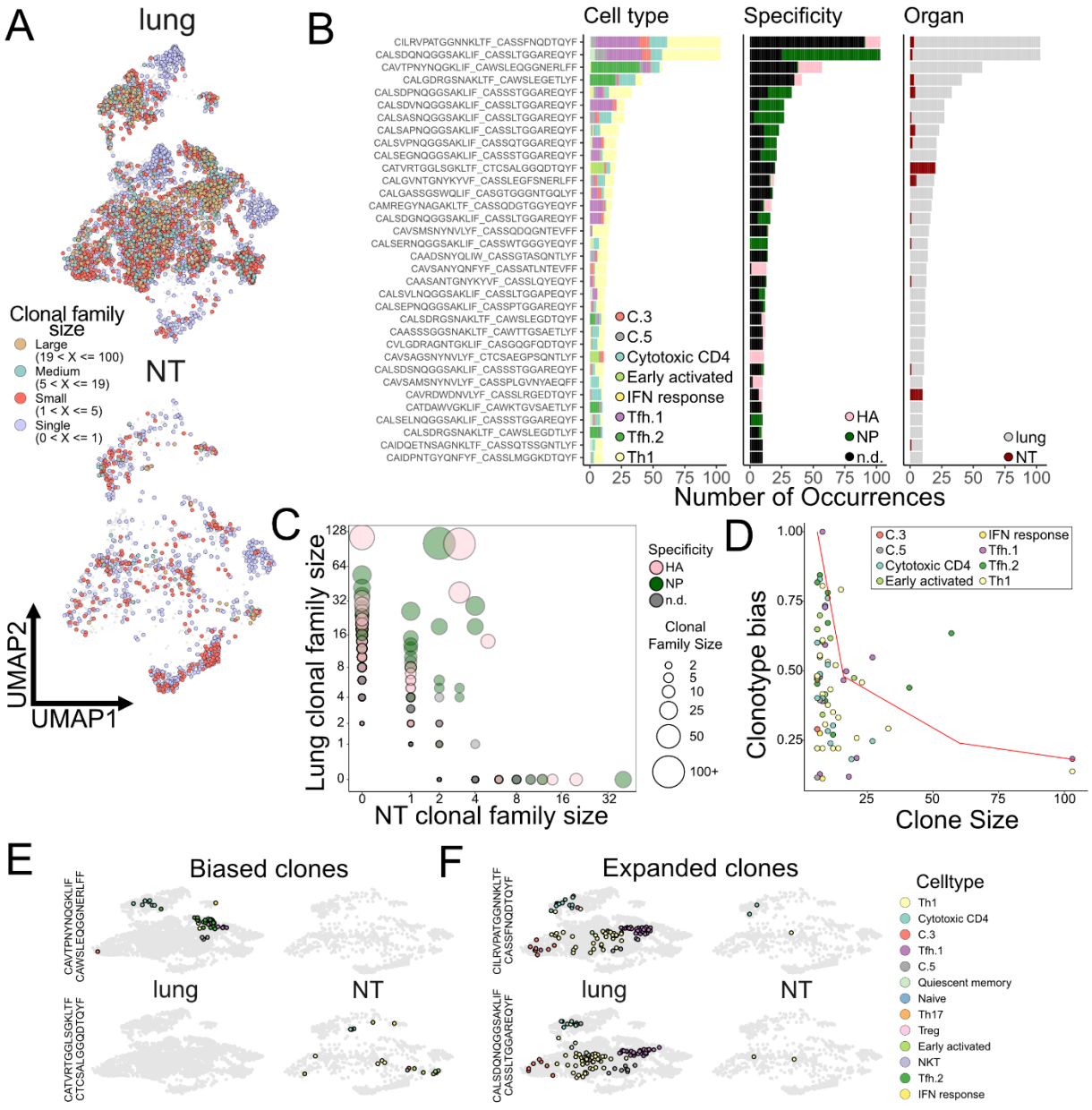

Fig 4: Single cell TCR VDJ sequencing reveals antigen specific CD4 TRM clonal distribution within organs and cell clusters

A) UMAP plot split by tissue (lung or NT) and colored according to clone size for CD4 TRM in IAV infected mice. Clones were binned into single clones (1 member; light blue), small (2 to 5 members; red), medium (6 to 19 members; green), large (over 20 members; gold). Light grey dots represent cells where TCR clonotype could not be assigned.

B) Bar plot characterizing the top 34 most expanded clones. The y axis reports CDR3 sequences of TCRαβ while the bar graphs show the number of cells divided according to cluster distribution, I-A^b $NP_{306-322}$ tetramer$^+$ or I-A^b HA_{91-107} tetramer$^+$ and organ specificity. n.d. = not determined.

C) Graph showing clonal relationship between lungs and NT from PR8 IAV infected mice. Each circle indicates one clonal family and size of the circle defines the size of the clonal family. Color of the circle denotes the antigenic specificity against I-A^b $NP_{306-322}$ tetramer and against I-A^b HA_{91-107} tetramer. n.d. = not determined.

D) Clonotype bias plot for clones with at least 6 cells. Clonotypes are colored according to predominant cluster. The red line highlights the null distribution (background distribution) for each clone size. The clones to the right of the red line are biased clones.

E) UMAP plot, split by tissue (lung or NT), depicting two biased clones. Cells belonging to the clonal family are colored according to the cluster while other cells are in light grey.

F) UMAP plot, split by tissue (lung or NT), depicting the two most expanded clones. Cells belonging to the clonal family are colored according to the cluster while other cells are in light grey.

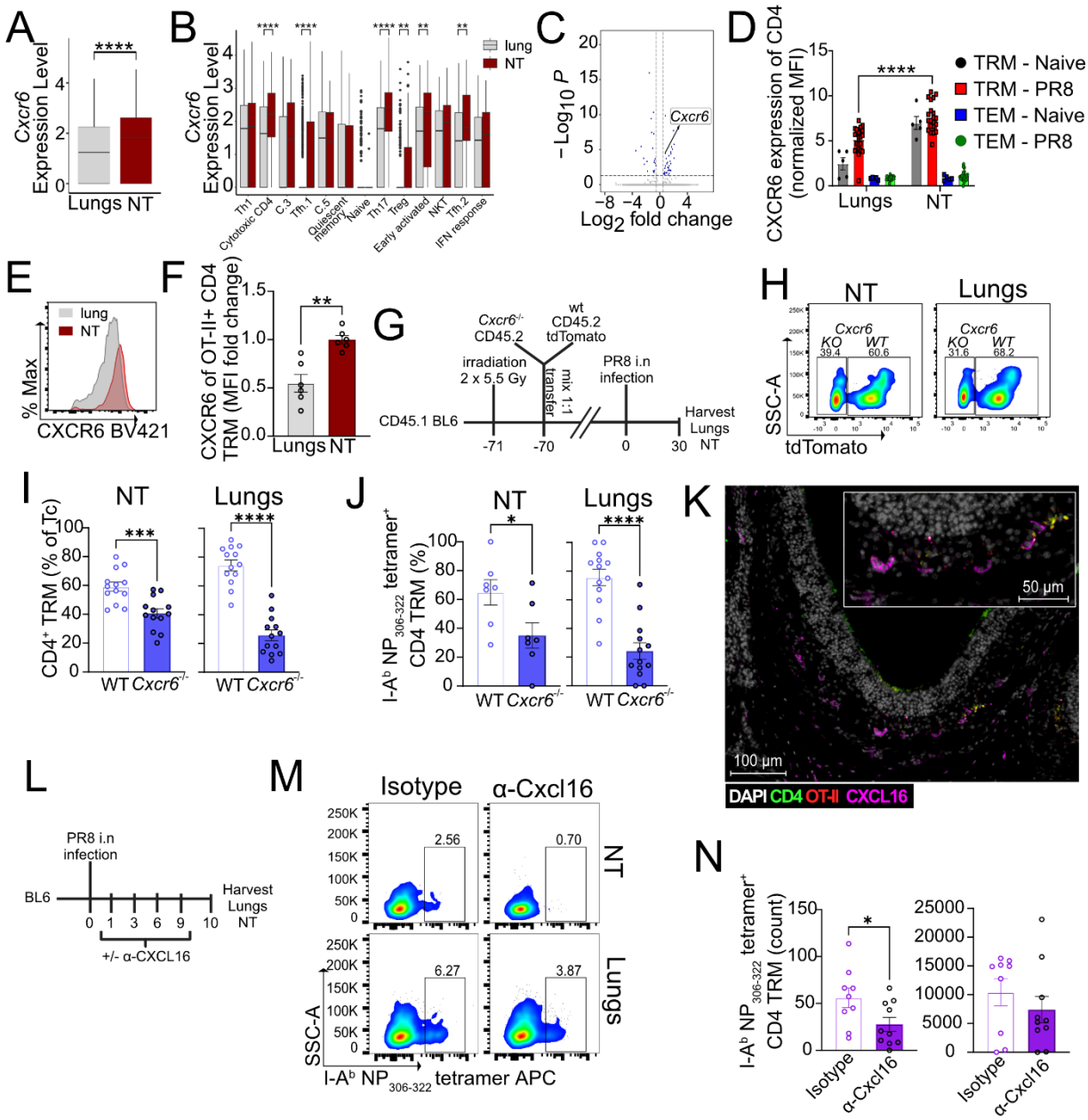

Fig 5: NT CD4 TRM rely on CXCR6-CXCL16 axis for their formation

A) Box plot showing the expression of *Cxcr6* mRNA among CD4 TRM of the NT and lungs. Data are presented as median and interquartile range. NS, not significant, ****P<0.0001; ***P<0.001; **P<0.01; *P<0.05 by unpaired two-tailed t-test.

B) Box plot showing the expression of *Cxcr6* mRNA among different cell clusters of lungs and NT. Data are presented as median and interquartile range. NS, not significant, ****P<0.0001; ***P<0.001; **P<0.01; *P<0.05 by Wilcoxon rank sum test with Benjamini-Hochberg correction

C) Volcano plot for differential expressed genes in the NT in comparison to the lungs of the Th17 cluster. The dotted lines indicate fold change and adjusted p value cutoffs.

D) Bar plot for the expression of CXCR6 (each Median Fluorescence Intensity (MFI) normalized to mean MFI from CD4 TEM iv^+ of NT) in CD4 TRM and iv^+ CD4 TEM from the lungs and NT of naïve mice and PR8 IAV infected mice (30 dpi) as indicated. The experiment was repeated thrice and the results (mean ± s.e.m.) are pooled. NS, not significant, ****P<0.0001; ***P<0.001; **P<0.01; *P<0.05 by two-way ANOVA, with Tukey's multiple comparison test.

E-F) Expression of CXCR6 on OT-II CD4 TRM of NT and lung on d30 following PR8-Ova infection as indicated. E) Representative histograms for CXCR6 expression from OT-II CD4 TRM of NT and lung are shown. F) Scatter plot showing the expression of CXCR6 (each Median Fluorescence Intensity (MFI) normalized to mean MFI of NT OT-II CD4 TRM). The experiment was repeated thrice and the results (mean ± s.e.m.) are pooled. NS, not significant, ****P<0.0001; ***P<0.001; **P<0.01; *P<0.05 by unpaired two-tailed t-test.

G-J) Frequency of different cell populations within different organs derived from WT- *Cxcr6*$^{-/-}$ BM chimeric mice on day 30 post infection with PR8 IAV as indicated. G) Schematic representation of the experimental setup. H) Representative flow cytometry plots showing the percentage of WT and *Cxcr6*$^{-/-}$ CD4 TRM in NT and lungs. I) Scatter plot for the percentage of WT and *Cxcr6*$^{-/-}$ CD4 TRM in NT and lungs as indicated. J) Scatter plot for the percentage of I-A^b $NP_{306-322}$ tetramer - specific WT and *Cxcr6*$^{-/-}$ CD4 TRM in NT and lungs as indicated. The experiment was repeated thrice and the results (mean ± s.e.m.) are pooled. NS, not significant, ****P<0.0001; ***P<0.001; **P<0.01; *P<0.05 by unpaired two-tailed t-test.

K) A representative microscopic image of CXCL16 expression (magenta) and OT-II CD4 T cells (red and green) in the olfactory epithelium of the murine NT. NT is isolated on day 30 post PR8-Ova infection from mice that received OT-II CD4 T cells.

L-N) Antigen-specific CD4 TRM in the lungs and NT of mice treated with isotype control or anti-CXCL16 antibody on day 10 post PR8 IAV infection. L) Schematic representation of the experimental setup. M) Representative flow cytometry plots indicating the percentage of I-A^b $NP_{306-322}$ tetramer - specific CD4 TRM are shown. N) Scatter plot indicating the absolute number of I-A^b $NP_{306-322}$ tetramer - specific CD4 TRM. The experiment was performed twice and the results (mean ± s.e.m.) are pooled. NS, not significant, ****P<0.0001; ***P<0.001; **P<0.01; *P<0.05 by unpaired two-tailed t-test.

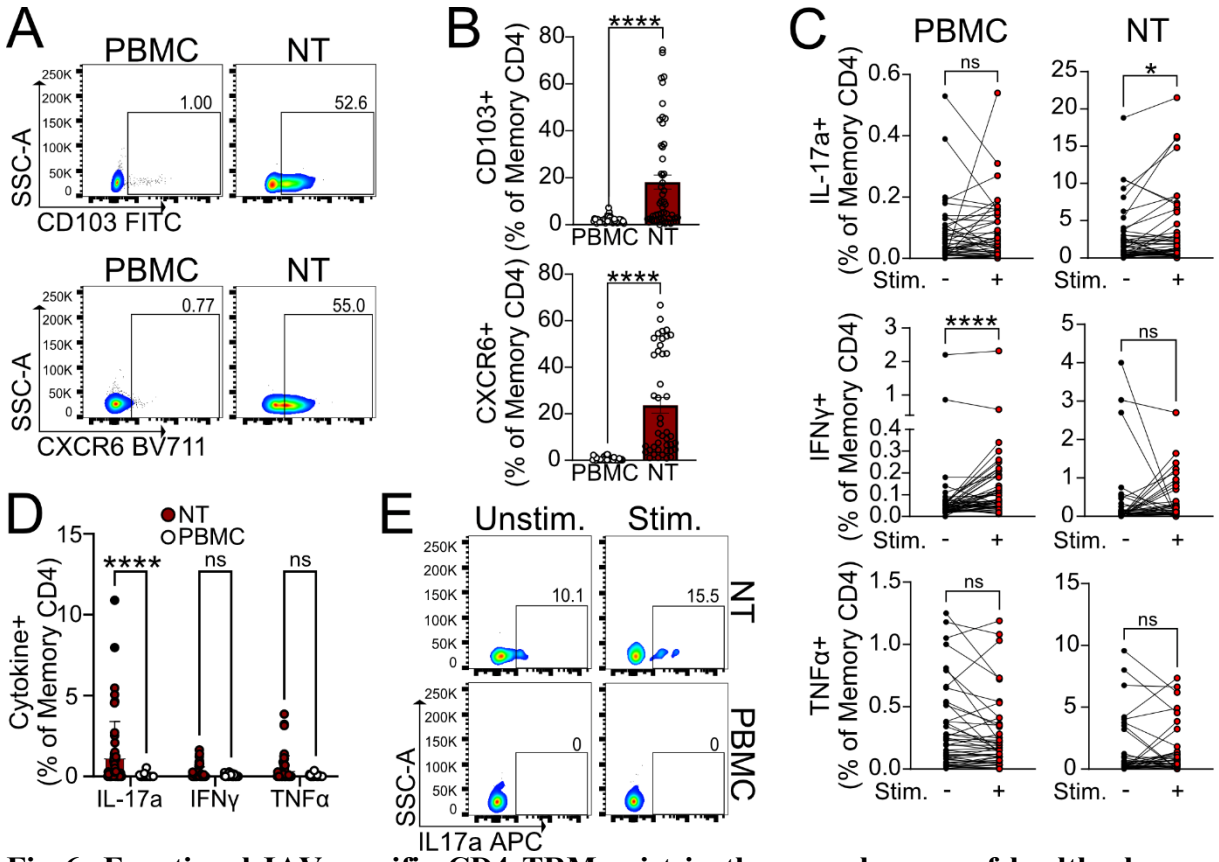

Fig 6: Functional IAV-specific CD4 TRM exist in the nasopharynx of healthy human subjects

A-B) Expression of CD103 and CXCR6 on NT CD4 TRM and CD4 TEM of PBMC derived from healthy human subjects. A) Representative flow cytometry plots indicating the percentage of CD103 and CXCR6 expression on CD4 TRM and CD4 TEM from the same subject. B) Scatter plot showing the percentage of CD103 and CXCR6 expression on CD4 TRM and CD4 TEM. Each data point indicates one subject. The experiment was performed five times and the results (mean ± s.e.m.) are pooled. NS, not significant, ****P<0.0001; ***P<0.001; **P<0.01; *P<0.05 by unpaired two-tailed t-test.

C) Percentage of NT CD4 TRM and CD4 TEM from PBMC expressing IL-17a, IFN-γ and TNFα. The cytokine expression is indicated from unstimulated cells and IAV NP peptide pool and M1 peptide pool stimulated cells connected by a line. Each line on the graph indicates cytokine expression from the cells of each subject. NS, not significant, ****P<0.0001; ***P<0.001; **P<0.01; *P<0.05 by two-sided Wilcoxon matched-pairs signed-rank test.

D) Scatter plot showing the percentage of NT CD4 TRM and CD4 TEM from PBMC expressing IL-17a, IFN-γ and TNF after stimulation with IAV NP peptide pool and M1 peptide pool (after subtraction of signals from the unstimulated control; negative values considered zero). The experiment was performed seven times and the results (mean ± s.e.m.) are pooled. NS, not significant, ****P<0.0001; ***P<0.001; **P<0.01; *P<0.05 by two-way ANOVA, with Tukey's multiple comparison test.

E) Representative flow cytometry plots showing the expression of IL-17a in NT CD4 TRM and CD4 TEM of PBMC which are stimulated with IAV NP peptide pool and M1 peptide pool or left unstimulated.

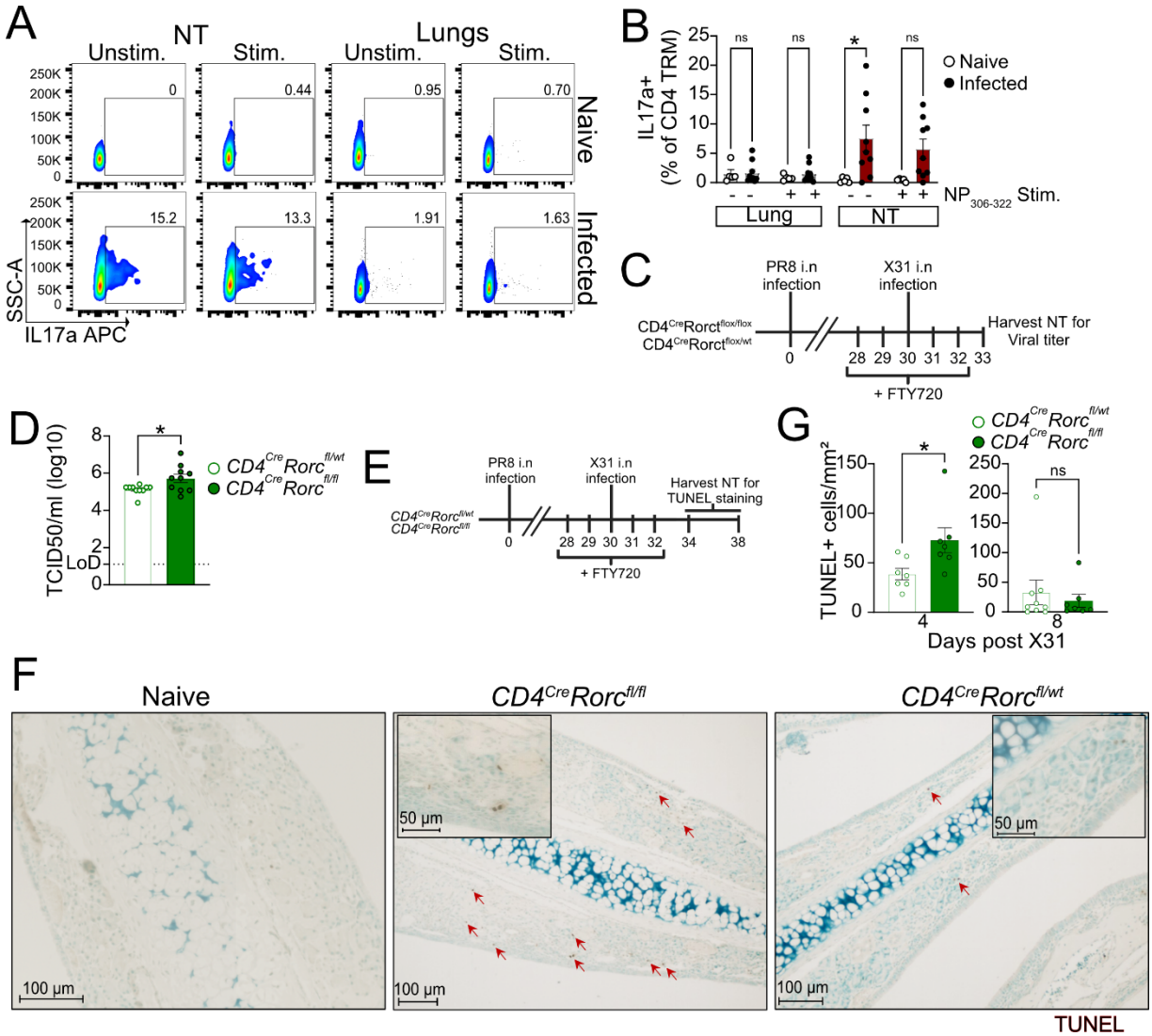

Fig 7: NT harbors protective IL-17a producing CD4 TRM population

A-B) Frequency of IL-17a^{+} cells among CD4 TRM of NT and lungs upon restimulation with IAV immunodominant $NP_{306-322}$ peptide in comparison to unstimulated cells. The organs

are isolated on day 30 following PR8 IAV infection of mice and from naïve mice. A) A representative flow cytometry plot showing the percentage of IL-17a in lungs and NT. B) Scatter plot indicating the frequency of IL-17a+ cells among all CD4 TRM. The experiment was repeated twice and the results (mean ± s.e.m.) are pooled. NS, not significant, ****P<0.0001; ***P<0.001; **P<0.01; *P<0.05 by two-way ANOVA, with Tukey's multiple comparison test.

C-D) Viral titers in the NT of *CD4*^{cre}*Rorct*$^{fl/fl}$ and *CD4*^{cre}*Rorc*$^{fl/wt}$ mice on day 3 following secondary infection with X31 IAV. The mice were infected with PR8 and reinfected with X31 IAV on day 30 post primary infection and treated with fingolimod ip as indicated. C) A schematic representation of the experimental setup. D) Scatter plot showing viral titers (TCID50/ml) in the NT of the two groups. The experiment was repeated twice and the results (mean ± s.e.m.) are pooled. NS, not significant, ****P<0.0001; ***P<0.001; **P<0.01; *P<0.05 by unpaired two-tailed t-test.

E-G) Microscopy for TUNEL^{+} cells in the nasal septum (respiratory region) derived from *CD4*^{cre}*Rorct*$^{fl/fl}$ and *CD4*^{cre}*Rorc*$^{fl/wt}$ mice. The mice were infected with PR8 and reinfected with X31 IAV on day 30 following PR8 IAV infection. The tissues were isolated on day 4 and day 8 following X31 IAV infection. E) A schematic representation of the experimental setup. F) Representative microscopic images for TUNEL^{+} cells (brown) in the nasal septum from mice on day 4 post X31 IAV infection are shown. Scale bar: 100µm. G) Scatter plot showing the number of TUNEL^{+} cells per mm2 in the respiratory region of the nasal septum. The experiment was repeated twice and the results (mean ± s.e.m.) are pooled. NS, not significant, ****P<0.0001; ***P<0.001; **P<0.01; *P<0.05 by two-way ANOVA, with Tukey's multiple comparison test.